TR-O-0085

49

Piezoelectric effect in InGaAs/GaAs quantum wells grown on (n11)A-oriented GaAs substrates (n=1, 2, 3, 4)

Pablo O. Vaccaro

1995. 4. 12

ATR光電波通信研究所

Piezoelectric effect in InGaAs/GaAs quantum wells grown on (n11)A-oriented GaAs substrates (n=1, 2, 3, 4)

Pablo O. Vaccaro

ATR

Optical and Radio Communications Research Laboratories
2-2 Hikaridai, Seika-cho, Soraku-gun, Kyoto 619-02, Japan

Contents

Abstract

Strained quantum wells (SQWs) of InGaAs play an important role in laser diodes, optical modulators and many other optoelectronic devices. These SQWs have been usually made on GaAs (100)–oriented substrates and do not show piezoelectric effect because crystal symmetry. We have grown InGaAs SQWs on GaAs (111)A, (211)A, (311)A, and (411)A–oriented substrates. High quality SQWs where obtained on GaAs (311)A and (411)A–oriented substrates. Moreover, (311)A–oriented SQWs showed an enhanced photoluminescence (PL) intensity, as compared to the (100)–oriented ones, suitable for laser diode applications. The built–in electric field generated by the piezoelectric effect in (311)A–oriented SQWs was also studied. In contrast to SQWs grown on (100)–oriented substrates, the PL excitation spectrum shows transitions that are forbidden in the absence of an electric field and the emergence of new energy levels confined by the tilted barrier in the hole bands.

InGaAs SQWs grown on GaAs (111)A–oriented substrates show strain relaxation even for layers below the predicted critical thickness. A strain relaxation mechanism peculiar to this surface was found. We made *pin* diodes with SQWs grown on GaAs (111)A 5° off–oriented substrates. The PL spectrum shows the influence of the piezoelectric field. We demonstrate the blueshift of the PL peaks with applied bias and propose a bistable device using this effect.

Finally, temporal variations of the PL peak wavelength due to screening of the piezoelectric field by photogenerated carriers were studied in undoped samples by using time–resolved and wavelength–resolved measurements of the PL intensity decay. The partial screening of the piezoelectric field by photogenerated carriers shifts the PL peak to shorter wavelengths and increases the oscillator strength. Results are explained using a model based on rate equations of photogenerated carriers and a recombination probability which is a function of the screened electric field.

KEYWORDS: InGaAs, (111)A, (211)A, (311)A, (411)A, substrate orientation, strained layer, photoluminescence, quantum well, piezoelectricity, molecular beam epitaxy.

Chapter I

Introduction

The growth of III–V semiconductor heterostructures on polar surfaces (i.e., (111), (211), (311), etc. orientations) of GaAs substrates is becoming an active field, since better crystal quality is being obtained and new applications are emerging[1),2)]. In particular, research on InGaAs/GaAs quantum wells grown on polar GaAs surfaces is attracting considerable attention because the presence of strain–induced electric fields could be useful for improving existing optoelectronic devices or developing completely new ones[3),4)].

The InGaAs quantum wells are also attractive as active layers of vertical–cavity surface emitting lasers (VCSELs) because lower threshold currents are obtained as compared to GaAs active layers. Besides, when the active layer is InGaAs, the distributed Bragg reflectors (DBRs), which are a key component of the VCSEL, can be made with alternating layers of AlAs and GaAs, and the required reflectivity is reached with fewer periods than in the case of GaAs active layers, were GaAs cannot be used in the DBRs because absorption. This difference becomes more notable when the maximun Al composition is limited by some other factor like surface smoothness on (111)A oriented GaAs. Figure 1.1 shows transmittance versus number of periods for DBRs that have the Al composition limited to 0.5. The DBR designed for InGaAs active layer reaches a reflectivity of 99% with only 27 periods as compared with the 33 periods that requires the DBR designed for a GaAs active layer.

InGaAs/GaAs devices that take advantage of the piezoelectric field have been grown only on (111)B surfaces up to now. The growth of InGaAs on (n11)A and B surfaces is a challenge. The most usual problems are relaxation of strain below calculated critical thickness, poor surface morphology, enhanced In surface segregation and twinning[5),6)].

The GaAs (111)A just oriented surface seems to be specially problematic, but on the other hand it has a very interesting property: Si behaves as an amphoteric dopant in GaAs epilayers grown on this surface, and very high p–type doping concentration with negligible compensation is obtainable. Besides, Si shows a very low diffusion coefficient as compared with the traditional p–type dopant, beryllium[7)].

The (111)A oriented substrates have another interesting feature. The piezoelectric field in the InGaAs layer can be used to produce or to enhance a two–dimensional electron gas (2–DEG) at the heterointerface.[4)] The 2–DEG in quantum wells grown on B surfaces is formed at the second interface in the growth

order as shown in Fig. 1.2. This interface is usually rougher than the first interface and a poorer electron mobility can be expected. On the othe hand, the 2-DEG is formed at the first interface when using A surfaces, and better mobility can be expected.

Taking in consideration the scarce data available about InGaAs strained-layer quantum wells grown on these GaAs (n11)A oriented surfaces, and starting from the experience accumulated during the growth of GaAs and AlGaAs on these surfaces, we have grown InGaAs/GaAs quantum wells on various substrate orientations and studied their optical properties.

This report has the following structure:

Chapter II describes the growth of $In_{0.2}Ga_{0.8}As/GaAs$ quantum wells on GaAs (111)A exactly oriented and misoriented substrates. The dependence of strain relaxation on substrate orientation is studied in this section using PL spectroscopy. High quality samples with narrow PL peaks are obtained on GaAs substrates misoriented 5° toward [100]. Quantum well structures with AlGaAs carrier-confinement barriers suitable for active layers of laser diodes are also grown on (411)A, (311)A, (211)A and (111)A substrates. In particular, the (311)A sample shows strong PL peaks with 25 meV FWHM at room temperature.

In Chapter III the influence of the piezoelectric effect on the energy levels of InGaAs/GaAs single quantum wells grown on GaAs (311)A substrates is studied. The PL excitation (PLE) spectrum shows transitions forbidden in the absence of piezoelectric field and the emergence of new bounded energy levels.

Chapter IV shows the control of the energy levels in the InGaAs/GaAs quantum wells grown on GaAs (111)A substrates by applying an external voltage bias. A blueshift of the PL peak is obtained in a $p-i-n$ diode by increasing reverse voltage bias. This effect has important applications in optical switching and nonlinear optics.

Chapter V presents a study of the carrier dynamics in a InGaAs/GaAs single quantum well grown on a GaAs (111)A substrate. Temporal dependence of piezoelectric field screening by photogenerated carriers is studied using time-resolved PL spectroscopy. We present a model which is based on rate equations of photogenerated carriers and time dependent recombination probabilities. This model explain succesfully the experimental results.

References to chapter I

1) T. Yamamoto, M. Inai, M. Hosoda, T. Takebe, and T. Watanabe: Jpn. J. Appl. Phys. **32**, 4454, (1993).

2) K. Kobayashi, T. Takebe, T. Yamamoto, M. Fujii, M. Inai and D. Lovell: J.

Electron. Mater. **22**, 161, (1993).
3) A. S. Pabla, J. L. Sanchez–Rojas, J. Woodhead, R. Grey, J. P. R. David, G. J. Rees, G. Hill, M. A. Pate and P. N. Robson: Appl. Phys. Lett. **63**, 752, (1993).
4) E. S. Snow, B. V. Shanabrook and D. Gammon: Appl. Phys. Lett. **56**, 758, (1990).
5) A. M. Dabiran, P. I. Cohen, J. E. Angelo and W. W. Gerberich: Thin Solid Films **231**, 1, (1993).
6) M. Ilg and K. H. Ploog: Phys. Rev. **B48**, 11512, (1993).
7) A. Shinoda, T. Yamamoto, M. Inai, T. Takebe and T. Watanabe: Jpn. J. Appl. Phys. **32**, L1374, (1993).

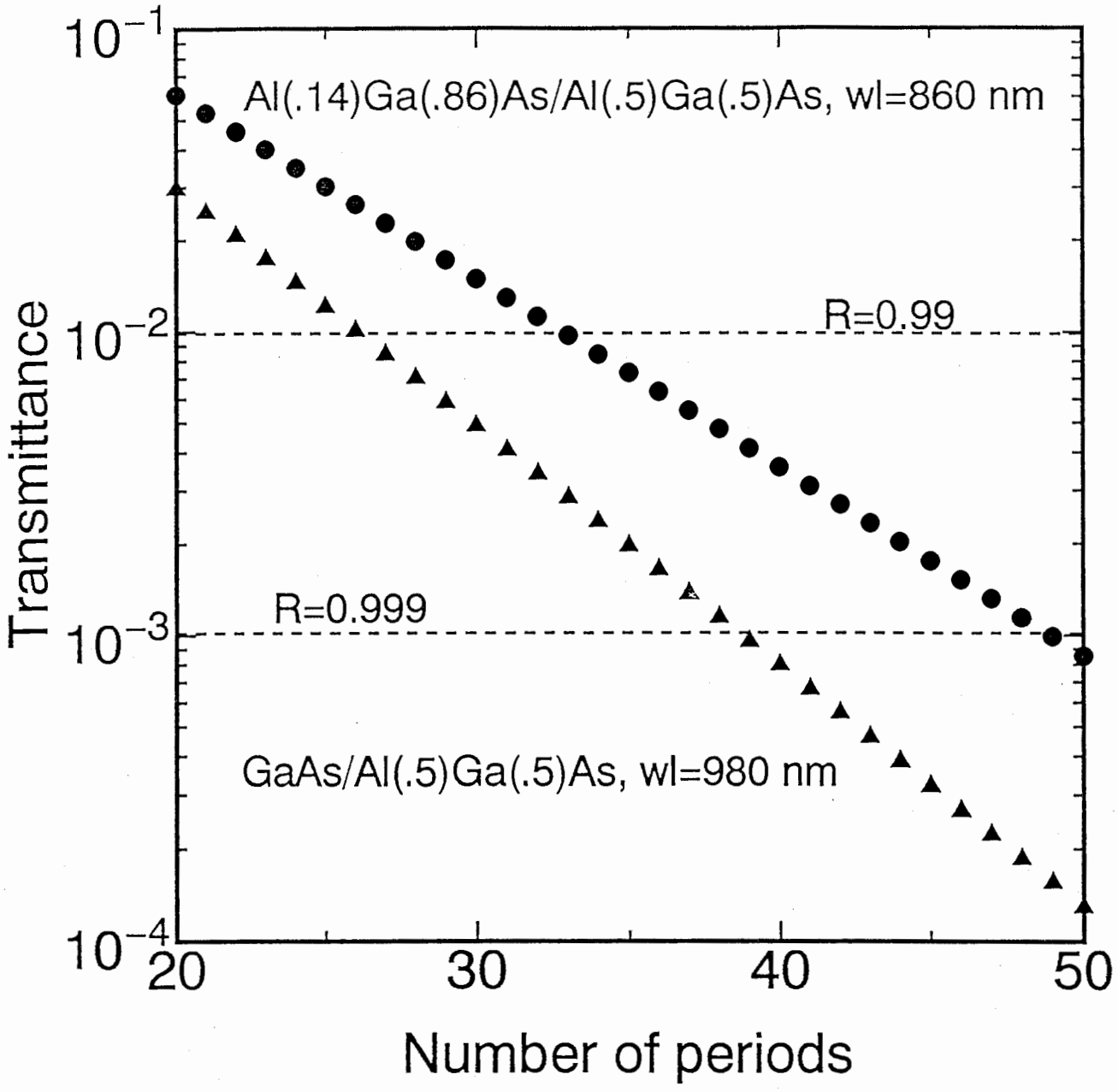

Figure 1.1: Transmittance of distributed Bragg reflectors designed for VCSELs with InGaAs and GaAs active layers. The calculation was performed assuming that the maximum Al fraction which can be used is 0.5.

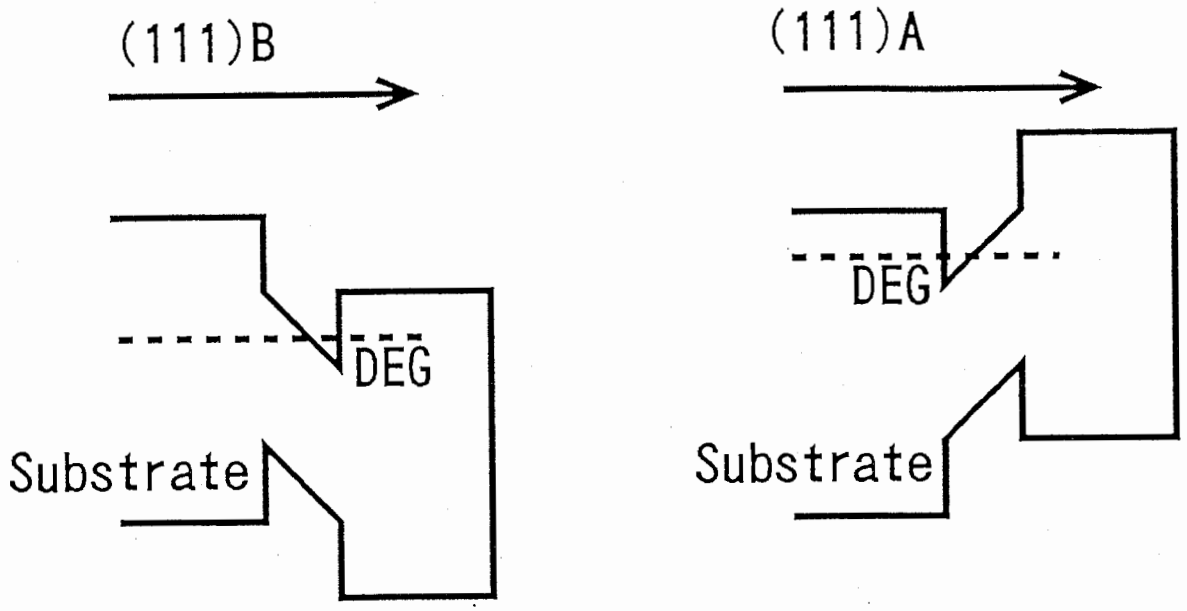

Figure 1.2: Two-dimensional electron gas formed using the piezoelectric effect on GaAs (111)A and (111)B-oriented substrates. The electron gas in the (111)A sample is formed at the interface nearer to the substrate which is smoother. A larger electron mobility is predicted as compared to the (111)B sample.

Chapter II

Growth by molecular beam epitaxy and strain relaxation

2.1. Sample preparation

InGaAs single quantum wells (SQW) were grown on semi-insulating GaAs substrates with the following orientations: (100), (111)A exactly oriented and (111)A misoriented 1° and 5° toward [001] and [110]. The native oxide layer was removed using H_2SO_4 and the wafers were rinsed in deionized water for 5 min. Subsequently the wafers were etched for 80 sec with $NH_4OH:H_2O_2:H_2O$ (2:1:95) at 25°C. After etching, the wafers were rinsed in deionized water for 5 min and dried with nitrogen. All samples were immediately mounted on molybdenum holders without indium and loaded into a Varian Modular Gen II MBE chamber. As_4 beam equivalent pressure was $2.2x10^{-5}$ Torr and the As_4/Ga flux ratio was 6.5. After thermal cleaning at 700°C for 5 min a 200 nm GaAs buffer layer was grown at 620°C. Substrate temperature was decreased during the last few minutes of GaAs growth before starting the growth of InGaAs at 560°C. The grown structure consisted of three (nominally) $In_{0.2}Ga_{0.8}As$ SQWs 10 nm, 5 nm and 2.5 nm thick separated by 50 nm GaAs barriers and a 50 nm cap layer (see Fig. 2.1). A set of samples with only one (nominally) $In_{0.15}Ga_{0.85}As$ SQW 5 nm thick was also grown.

Photoluminescence (PL) measurements were performed at 12K using an Ar^+ laser (488 nm wavelength) or a Ti-sapphire laser (844 nm wavelength), a monochromator and an InGaAs photomultiplier detector. The surface morphology of the samples was observed with a scanning electron microscope (SEM). One sample was also observed by transmission electron microscopy (TEM).

2.2. Photoluminescence peak energy

All the samples showed a smooth and featureless surface when observed with the SEM. In particular, we did not find the pyramid-shaped defects so usual in the (111)A oriented surfaces. It indicates the success of the pre-treatment and growth techniques used.

The InGaAs layers are biaxially compressed in the plane of the SQWs. This strain increases the bandgap and shifts the band alignment at heterointerfaces. The strained bandgap was calculated after Pollak[1]; band alignment was calculated using the solid model of Van de Walle[2] for (100) and (111)A surfaces. We

calculated the energy levels and wave functions by numerically solving the Schrödinger equation using the transfer matrix method. The values used in these calculations are given in Table I. The well thicknesses used in the calculation were obtained from the TEM measurement and they were coincident with the design values. The indium composition was obtained by fitting the calculated transition energies to the PL peak energies of the SQWs grown on the (100) substrate. We will assume that the SQWs grown on (111)A substrates have the same indium composition.

The PL peak energy of SQWs grown on (100) substrates coincides with the calculated e1–hh1 transition for completely strained InGaAs using an indium composition value x=0.18, as shown in Fig. 2.2. This composition is smaller than the nominal composition (x=0.20) because indium evaporation and segregation occur during the growth. On the other hand, the PL peak energy of SQWs grown on (111)A substrates shows a large redshift as compared with the calculated value for strained InGaAs without including the piezoelectric field (upper, short–dashed line in Fig. 2.3).

2.3. Piezoelectric effect

The strained InGaAs layer has a built–in electric field due to piezoelectric effect that tilts the band edges. This tilt localizes the electrons and holes in the opposite sides of the SQW and it also reduces the transition energy between energy levels in the conduction and valence band as shown in Fig. 2.4. This effect is called quantum–confined Stark effect (QCSE).

We calculated the strain generated electric field from bulk piezoelectric theory[3]. For x=0.18 on the (111) direction, the theoretical electric field is E=257 kV/cm. The long–dashed line in Fig. 2.3 shows the calculated transition energies for SQWs including this electric field. This line does not agree with the experimental results. We obtain a good agreement with the samples grown on GaAs (111)A 5° off toward [001] using an electric field 40% smaller (E=154 kV/cm) for the calculation (full line in Fig. 2.3). A surface charge density at the heterointerfaces of about $9x10^{-4}C/cm^2$ could be responsible for this reduction in the built–in electric field. The shift of the transition energies for the 10 nm, 5 nm and 2.5 nm SQWs is 64 meV, 18 meV and 3 meV respectively. The PL peak energies of the samples grown on the other substrate orientations do not coincide with the calculated values for any piezoelectric field intensity. Therefore, there is another cause for the larger redshift observed in these samples, for example, interface roughness or strain relaxation.

The piezoelectric field can be screened by carriers inside the SQW. These carriers can be generated by optical excitation of electron–hole pairs. In turn, the screening of the piezoelectric field will reduce the redshift of the excitonic transi–

tion. We chose the sample grown on (111)A 5° off toward [001] substrate to demonstrate the screening of the piezoelectric field. The excitation wavelength is 844 nm, then the electron–hole pairs are generated only inside the SQW and not in the GaAs barriers. Therefore, nearly all electron–hole pairs generated recombine inside the well. The slope of the log–log plot of the PL intensity dependence on the excitation intensity is approximately one. It means that radiative recombination predominates over non–radiative process. Sample heating at high excitation intensities is not expected because only a small fraction (less than 1%) of the laser beam is absorbed in the sample. Figure 2.5 shows the dependence of PL peak energy on excitation intensity for the SQWs grown on the (111)A 5° off toward [001] substrate. The PL peaks of the 10 nm and 5 nm SQWs show a blueshift with increasing excitation intensity as expected. The PL peak energies are shifted 19 meV and 4 meV respectively in this excitation intensity range. On the other hand, the 2 nm SQW does not show appreciable blueshift. The shifts of the 10 nm and 5 nm SQWs are appreciably smaller than the ones calculated in the previous paragraph. We think that this is due to the incomplete screening of the piezoelectric field because photogenerated carriers diffuse quickly outside the illuminated region.

2.4. Abnormal redshift of the PL peaks

The largest redshift observed in Fig. 2.3 corresponds to SQWs grown on GaAs (111)A 1° off toward [001] substrates and the smallest redshift corresponds to GaAs (111)A 5° off toward [001] substrates. The difference between these energies is about 50 meV. Since the piezoelectric effect has nearly the same intensity on both substrate orientations, the difference can not be attributed to the QCSE. Moreover, the thinner wells show an energy difference larger than the thicker wells. If the larger redshift in the 1° off samples is originated in stronger built–in electric field, the opposite behavior is expected.

Not only the piezoelectric effect but interface roughness (islanding) redshifts the energy peaks and increases FWHM. Recently Ping and Dalal[4] proposed a model that describes these effects. The model is based on the geometrical properties of the well and the thermal distribution of excitons in growth islands where the quantum well has different thickness. A Gaussian distribution of these islands is assumed. The FWHM of this Gaussian distribution is called interface fluctuation parameter and it shows the structural quality of the quantum well. Two limit situations are analytically tractable: (a) when the energy difference between adjacent islands is much larger or (b) much smaller than the thermal energy kT. The energy difference between large islands (as compared with the exciton diameter) differing in one monolayer for the 5 nm SQW on (111)A surface is 2.9 meV and kT for 12K is about 1 meV. We calculated the intensity of excitonic

peaks for each island thickness among 10 and 20 monolayers (1 monolayer of $In_{0.18}Ga_{0.82}As$ (111) is about 0.331 nm, therefore the 5 nm SQW is about 15 monolayers thick) using the first approximation. If the FWHM of PL peaks for each island thickness is wide enough (more than 2.9 meV), the individual peaks are not resolved and the peak shape observed will be the addition of the individual peaks. The intensity of the individual peaks is given by [4]

$$I \sim \exp\{[E(L_0)-E(L)]/kT\} \exp[-(L-L_0)^2/\sigma^2] \ , \qquad (2.1)$$

where E is the transition energy of a SQW with thickness L, L_0 is the average thickness of the actual SQW, kT is the exciton's thermal energy and σ is the interface fluctuation parameter.

Figure 2.6 shows the relationship between PL peak energy and FWHM for 5 nm SQWs grown on (111)A just and misoriented substrates. The model's result obtained for various values of interface fluctuation parameter is the line (a) in Fig. 2.6. The calculated redshift is very small as compared with the experimental data. This result can be explained as follows: if the islands are smaller than the exciton diameter, the excitons will see an averaged potential when moving in the well. Therefore, the energy barriers that excitons have to jump for moving in areas with higher potential energy could be much smaller than kT even at 12K and the second approximation of the model should be used. In this case, the PL intensity is given by[4]

$$I \sim \exp[-(L-L_0)^2/\sigma^2] \sum_{L'<L} \exp[-(L'-L_0)^2/\sigma^2] \ . \qquad (2.2)$$

Also in Fig. 2.6 the calculated values for the second approximation of the model are shown (line (b)). The calculated redshift is somewhat larger but it is smaller than the measured values. Furthermore, we observed the cross section of the sample grown on GaAs (111)A just substrate by TEM and we found that the variation in thickness of the SQWs is less than three monolayers. We conclude that the measured redshift can not be originated only from the interface roughness but there is also strain relaxation in these samples.

2.5. Strain relaxation

From the Matthews and Blackslee model[5], the critical thickness for a $In_{0.18}Ga_{0.82}As$ strained layer on the GaAs (111) surface is about 40 monolayers or 13.2 nm. Since the same model predicts a critical thickness about 27 monolayers or 7.7 nm on the GaAs (100) surface, we expected that thicker strained layers could be grown on the (111)A surfaces. Instead, we found the opposite situation: samples grown on (111)A surface show strain relaxation for thickness far below

the calculated critical thickness, and samples grown on (100) surfaces do not show strain relaxation even for samples with thickness larger than the critical thickness. We measured a dislocation density of about $1x10^{10}$ cm^{-2} in the sample grown on GaAs (111)A just oriented substrate when observed by TEM. This dislocation density produces about 20% of strain relaxation that is enough for explaining the observed redshift.

We were worried about the influence of the thicker wells (that were grown first) on the thinner wells (grown after these). If the thicker wells produce a rough interface, they could degrade the thinner wells. Reithmayer et al.[6] observed that even if an InGaAs layer produces a rough interface, the surface becomes flat again after growing the GaAs spacer. Then, the next InGaAs layer is not perturbed by the previous one. Their samples were grown on GaAs (100) substrates. In order to corroborate this effect on GaAs (111)A substrates, we grew samples with only one 5 nm SQW. The FWHM of the PL peak of these samples is equal to the PL peak of the 5 nm SQW in samples containing the three SQWs. From this observation we conclude that even if the thicker SQWs have a rough interface, the flatness of the surface is recovered while growing the GaAs spacer and the next SQW is not degraded.

Dabiran et al.[7] found an interesting phenomenon when growing $In_{0.28}Ga_{0.72}As$ on GaAs (111)B 0.5° off toward [110] at 400°C. Strain relaxation is observed as soon as growth is started, but considerable residual strain remains even for layers thicker than the critical thickness. On the other hand, they are able to grow $In_{0.34}Ga_{0.66}As$ strained layers up to 65 monolayers on GaAs (111)B 1° off toward [211] at 450°C.

Grandjean and Massies[8] showed that the growth front of InGaAs undergoes a 2D–3D transformation before dislocations start to be formed in the epilayer. This 3D surface has lower energy than the equivalent 2D surfaces because the edges of the islands are partially relaxed in a non–tetragonal fashion.

Orr et al.[9] simulated the growth of strained films using the Monte Carlo method. They found that from the onset of deposition the films are energetically unstable to large–scale islanding. They also show that islanding will appear even far below the Matthews–Blackslee calculated critical thickness if the adatom migration length is long enough.

We consider that our results are the experimental corroboration of this model. The adatom migration length under our growth conditions is larger on the (111)A surface than on the (100) surface[10]. Islands would be formed just after InGaAs growth starts. The coalescence of these islands will generate dislocations and the growth front will show islands with a height of few monolayers as observed by TEM.

Some of the 2.5 nm SQWs shown in Fig. 2.3 have PL peak energies smaller than the expected value for a completely relaxed SQW. Also the interface rough–

ness observed by TEM should be responsible for this effect. The islands are thicker than the SQW design thickness (2.5 nm). Then the quantum confinement energy decreases. This energy decrease and the strain relaxation originate the abnormal redshift.

It can be argued that the indium composition of the SQWs grown on GaAs (111)A and (100) substrates could be different. We calculated the SQWs' transition energies for both substrate orientations with various indium compositions to clarify this point. The calculated values showed that a change in the indium composition cannot explain the observed results.

The strain relaxation dependence on misorientation angle is not understood yet. GaAs (111)A 5° off have a larger step density that can reduce the adatom migration length. This reduction will delay island formation and strain relaxation. The same explanation, however, does not agree with the fact that (111)A 1° off SQWs show larger redshift than (111)A just SQWs.

2.6. Quantum wells with AlGaAs barriers

Samples with $Al_{0.35}Ga_{0.65}As$ carrier confinement barriers were grown on (100), (411)A, (311)A, (211)A and (111)A 5° off toward [100]-oriented GaAs substrates to evaluate the application of the $In_{0.2}Ga_{0.8}As$ SQWs as active layers in laser diodes. Figure 2.7 shows the potential profile that surrounds each quantum well in the structure. Figure 2.8 shows the low temperature PL spectra excited with 5 mW Ar^+ laser. The presence of the AlGaAs barrier prevents the diffusion and non-radiative recombination of carriers at the front surface, therefore the PL peak intensity of the 2.5 nm SQW, which is the closest to the surface, is the strongest due to the higher excitation intensity near the surface.

The peak energy of samples grown on (100) and (311)A substrates agree with calculated values using an indium composition of x=0.181. The 10 nm SQW of the sample grown and (111)A 5° off is redshifted, possibly due to strain relaxation.

Figure 2.9 shows the PL spectra of the same samples at room temperature, excited with 100 mW Ti-sapphire laser. In this case, the 844 nm laser light is only absorbed in the SQWs and GaAs spacers, and it is not absorbed in the AlGaAs barriers. Samples grown on (100) and (311)A substrates show intense and narrow PL peaks (FWHM about 25 meV). In particular, the sample grown on a (311)A substrate shows the best characteristic, with twice the intensity of samples grown on (100) substrate for the 5 nm SQW. The PL of the SQWs grown on the (111)A 5° off substrate is barely distinguishable, and the light emission comes mainly from the GaAs spacers. This fact is in agreement with the presence of partial strain relaxation and dislocations that are non-radiative recombination centers.

2.7. Conclusions

InGaAs/GaAs SQWs grown on GaAs (100), (111)A just and misoriented substrates have been investigated. Samples grown on GaAs (111)A just and misoriented substrates show large FWHM and redshift of the PL peaks as compared with calculated values.

The redshift observed in SQWs grown on a (111)A 5° off toward [001] substrate can be explained by the presence of a built–in electric field E=154 kV/cm due to piezoelectric effect. This electric field is 40% smaller than the theoretical value and the difference can be attributed to the presence of fixed charges at heterointerfaces.

Using a model we conclude that the existence of growth islands without strain relaxation is not enough for explaining the redshift observed in SQWs grown on the other GaAs (111)A substrates. Moreover, TEM measurements in a sample grown on GaAs (111)A just–oriented substrate show quite flat heterointerfaces and a dislocation density of $1x10^{10}$ cm^{-2}. This dislocation density produces about 20% of strain relaxation that is enough for explaining the observed redshift. However, the conventional strain relaxation mechanism should not be active because the SQW thickness is smaller than the critical thickness required for generation of misfit dislocations accordingly to the Matthews and Blackslee model[5].

A strain relaxation mechanism that includes non–tetragonal deformation of coherently grown islands when InGaAs growth begins and the generation of misfit dislocations when these islands coalesce gives a qualitative explanation of the observed results.

$In_{0.2}Ga_{0.8}As$/GaAs SQWs with AlGaAs barriers for carrier confinement were grown on (411)A, (311)A and (211)A GaAs substrates show interesting PL characteristics. In particular, samples grown on (311)A oriented substrates show strong PL at room temperature that is promisory for application in the active layer of laser diodes.

References to chapter II

1) F. H. Pollak: Semiconductors and Semimetals Vol. 32 (edited by R. K. Willardson and A. C. Beer, Academic Press, 1991), p. 17.
2) C. G. Van de Walle: Mat. Res. Soc. Symp. Proc. **102**, 565, (1988).
3) D. Sun and E. Towe: Jpn. J. Appl. Phys. **33**, 702, (1994).
4) E. X. Ping and V. Dalal: J. Appl. Phys. **74**, 5349, (1993).
5) J. W. Matthews and A. E. Blackslee: J. Crys. Growth **27**, 118, (1974).

6) J. –P. Reithmayer, H. Riechert and H. Schlotterer: J. Crys. Growth, **111**, 407, (1991).
7) A. M. Dabiran, P. I. Cohen, J. E. Angelo and W. W. Gerberich: Thin Solid Films **231**, 1, (1993).
8) N. Grandjean and J. Massies: J. Crys. Growth **134**, 51, (1993).
9) B. G. Orr, D. Kessler, C. W. Snyder and L. Sander: Europhys. Lett. **19**, 33, (1992).
10) K. Kobayashi, T. Takebe, T. Yamamoto, M. Fujii, M. Inai and D. Lovell: J. Electron. Mater. **22**, 161, (1993).

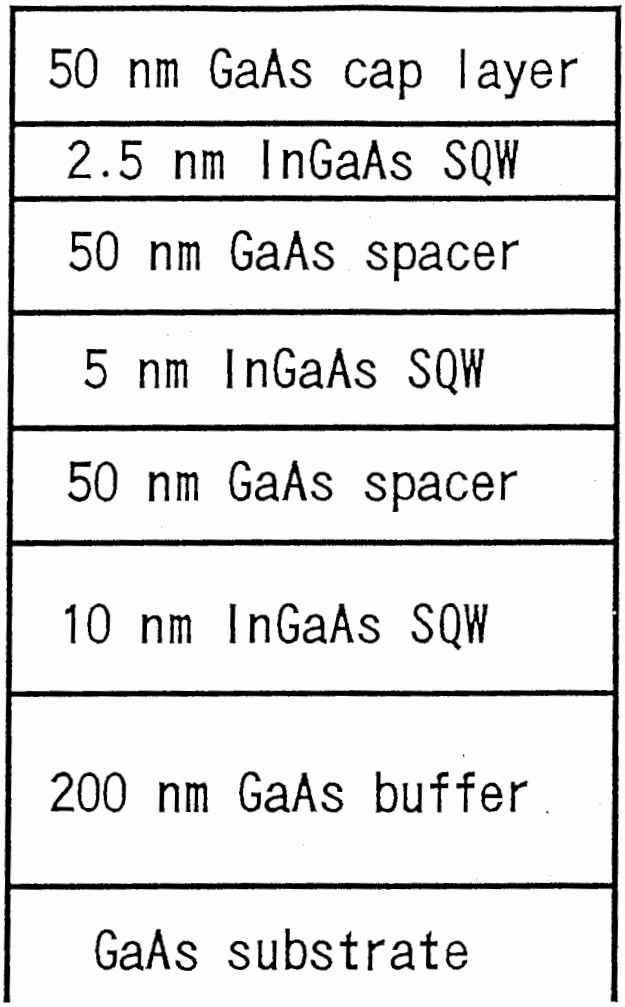

Figure 2.1: Structure of the samples. GaAs was grown at 620°C. InGaAs was grown at 560°C.

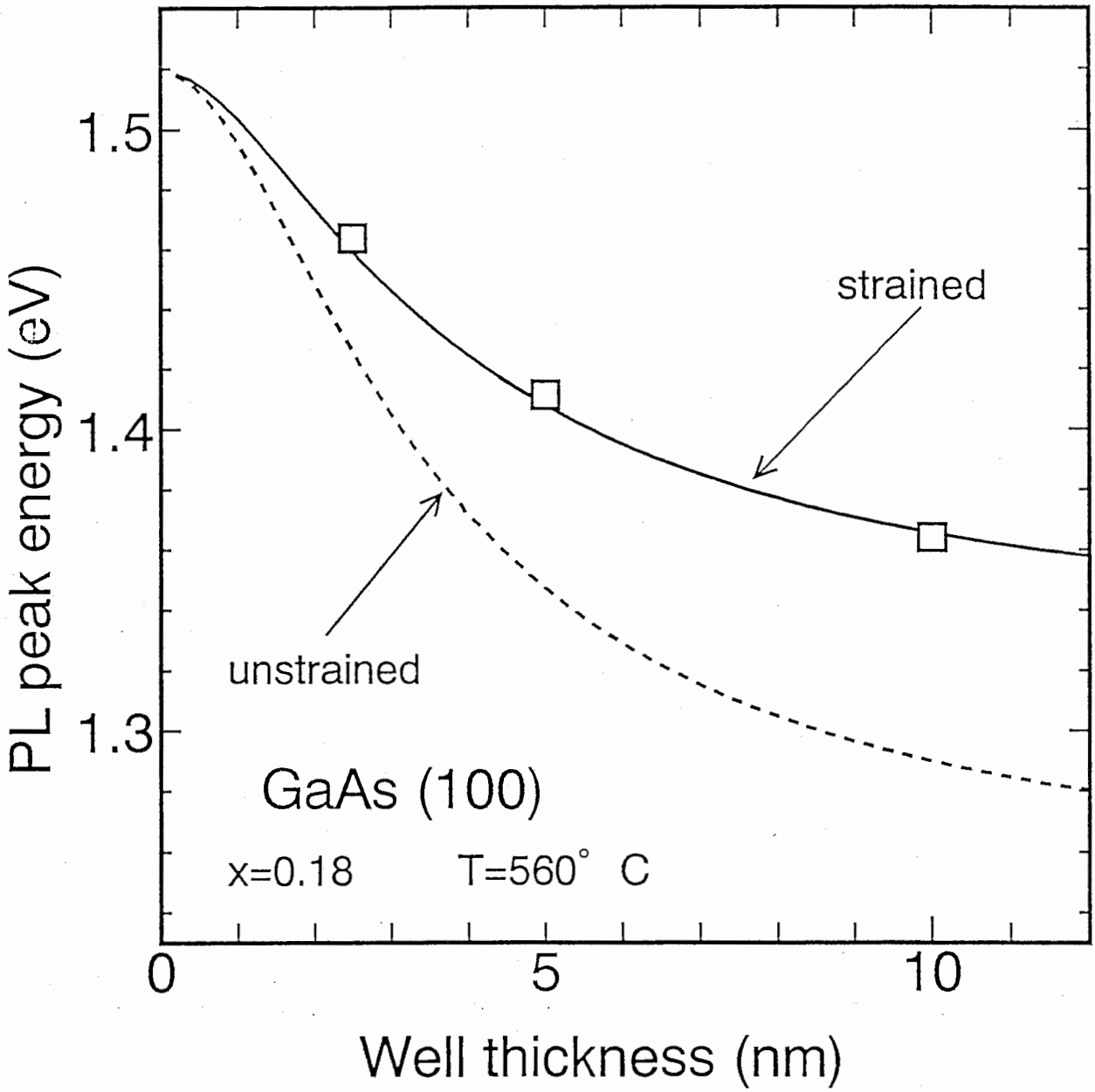

Figure 2.2: Photoluminescence peak energy dependence on well thickness for SQWs grown on GaAs (100) substrates. The solid (dashed) lines are the calculated transition energy for strained (relaxed) InGaAs.

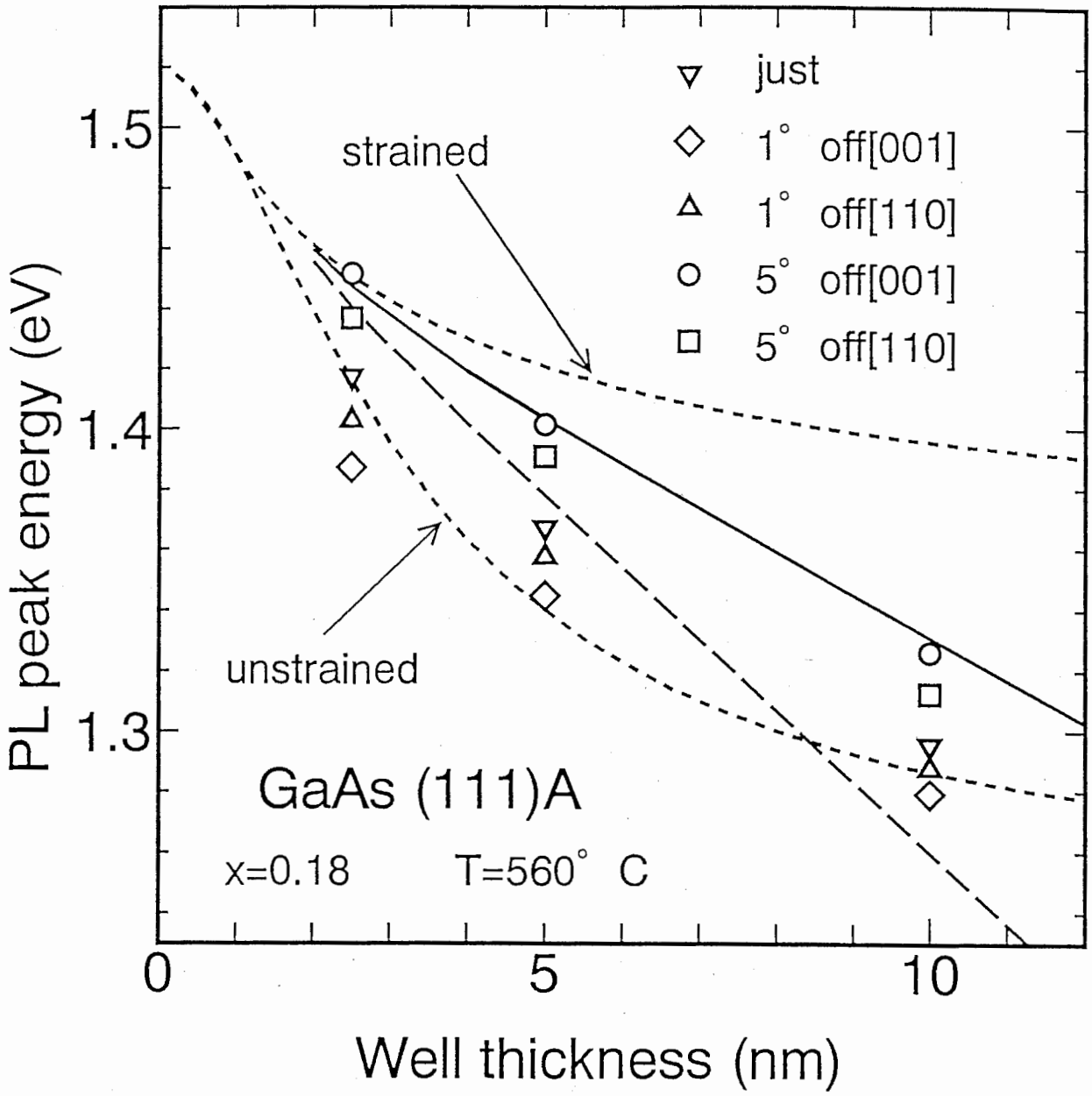

Figure 2.3: Photoluminescence peak energy dependence on well thickness for SQWs grown on GaAs (111)A substrates. The upper (lower) short–dashed line is the calculated transition energy for strained (relaxed) InGaAs without including the piezoelectric effect. The long–dashed line is calculated including the theoretical piezoelectric field (E=257 kV/cm). The solid line is calculated with a piezoelectric field E=154 kV/cm to fit the experimental data.

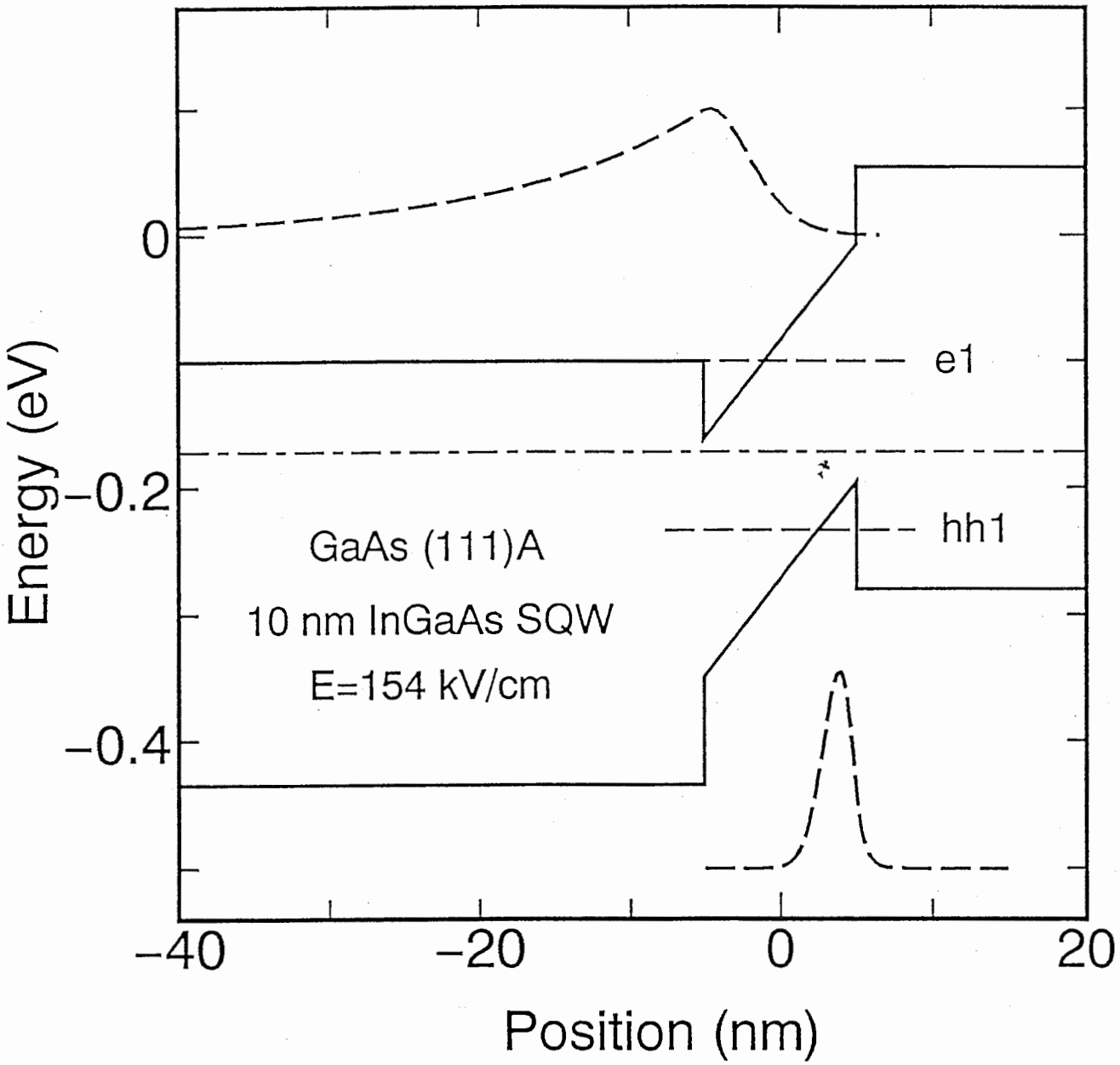

Figure 2.4: Potential profile for the 10 nm SQW grown on GaAs (111)A. The fundamental energy levels for electrons and holes and their wave functions are shown. The energy bandgap is not at the same scale.

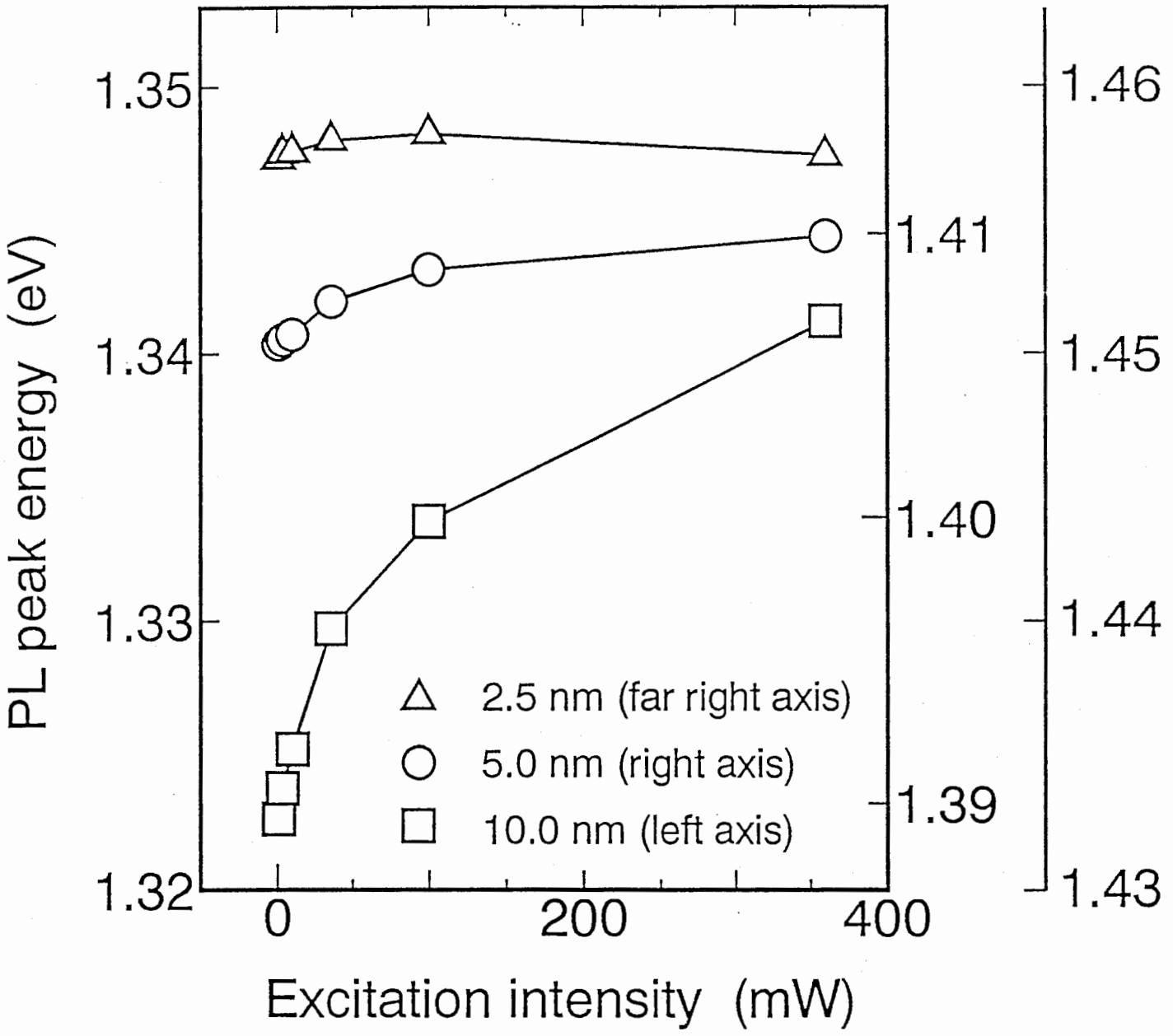

Figure 2.5: Photoluminescence peak energy dependence on excitation intensity for SQWs grown on GaAs (111)A 5° off [001] substrate measured at 12K. The excitation wavelength is 844 nm.

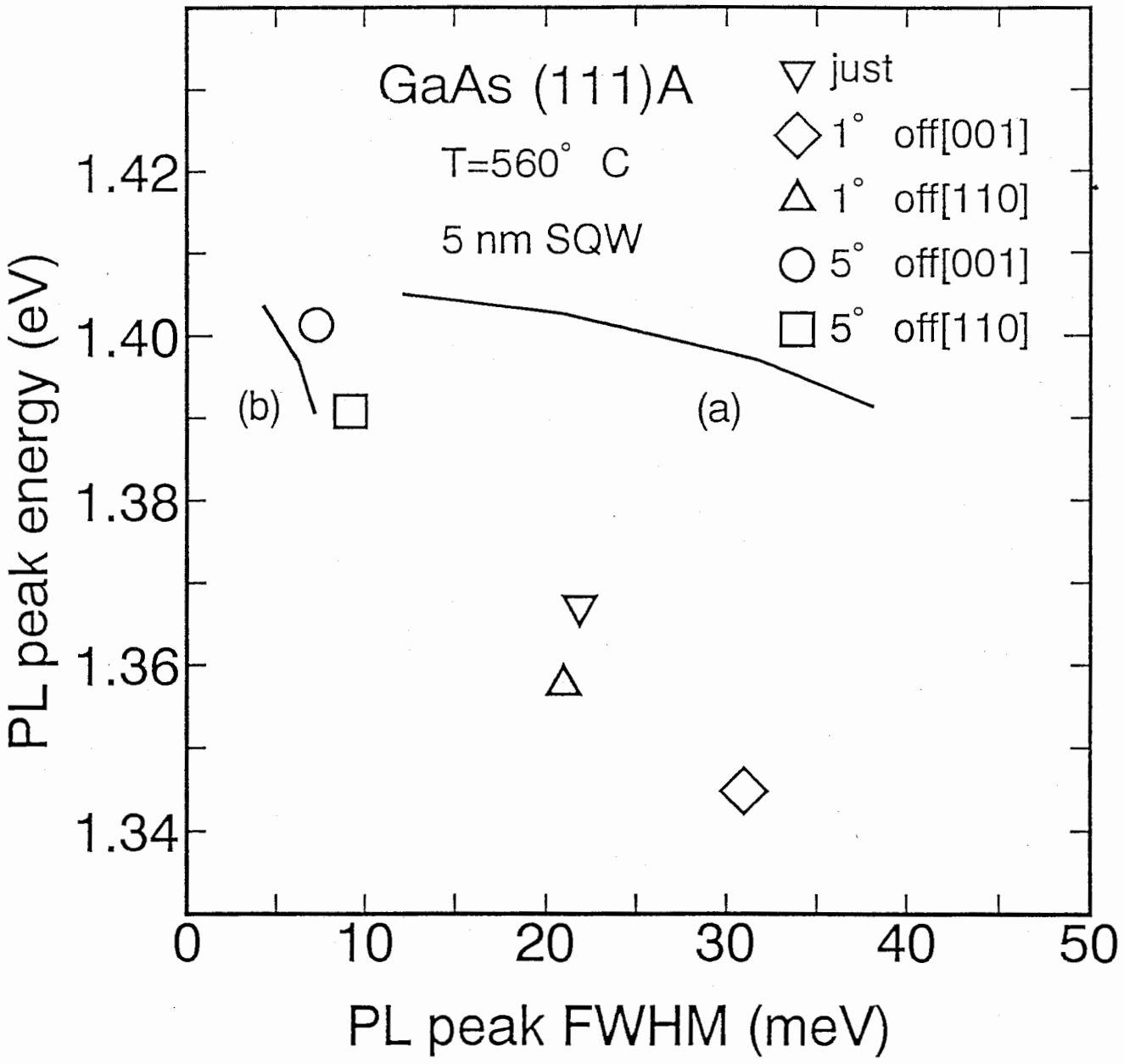

Figure 2.6: Relationship between PL peak energy and FWHM for 5 nm SQWs grown on (111)A just and misoriented substrates. Calculated lines: (a) First approximation. (b) Second approximation (see text for details).

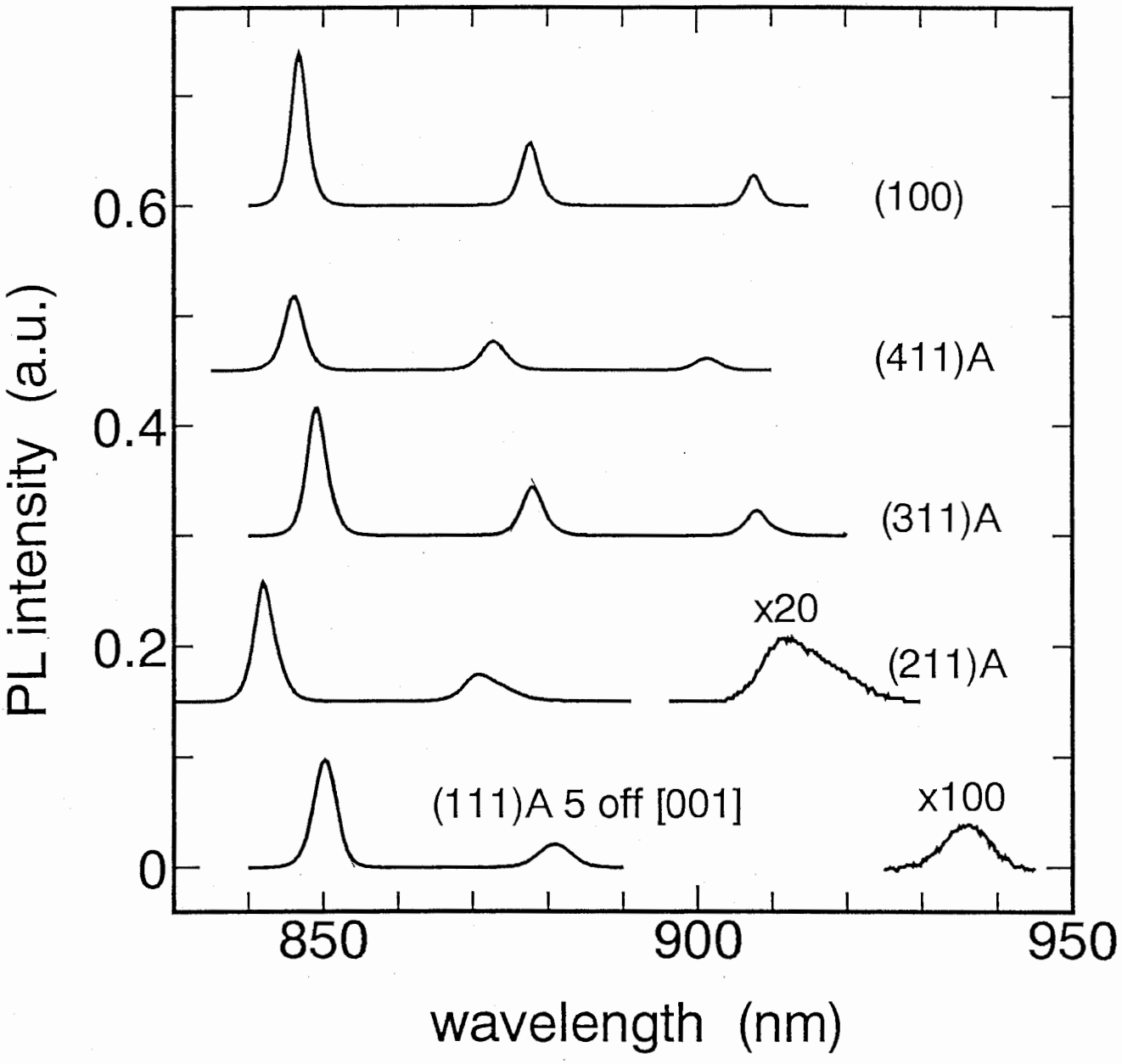

Figure 2.8: Photoluminescence spectra of samples with AlGaAs barriers for carrier confinement measured at 12K. The spectra are shifted vertically for clarity. Excitation: 488 nm, 5 mW.

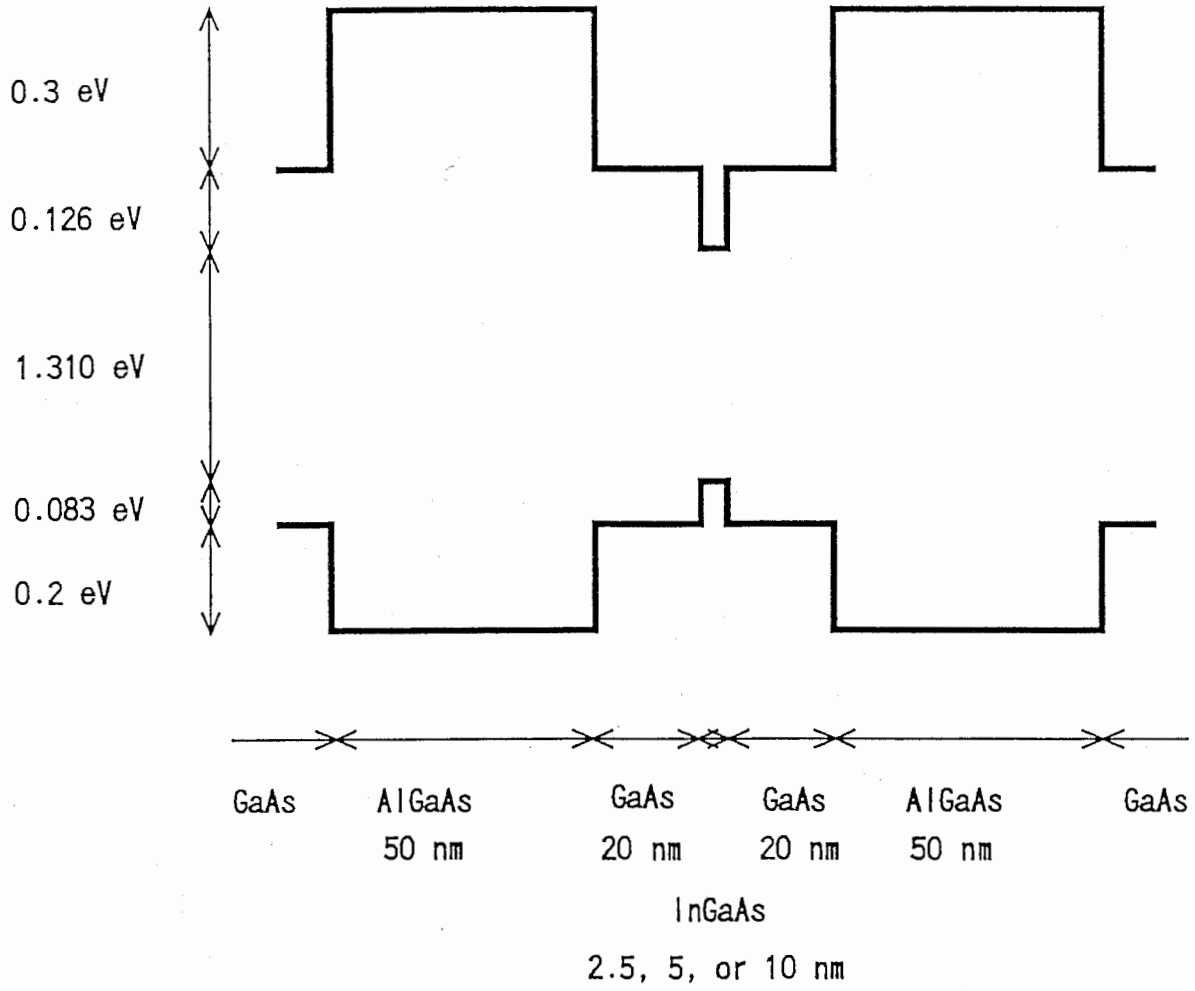

Figure 2.7: Potential profile surrounding the quantum wells that have AlGaAs barriers.

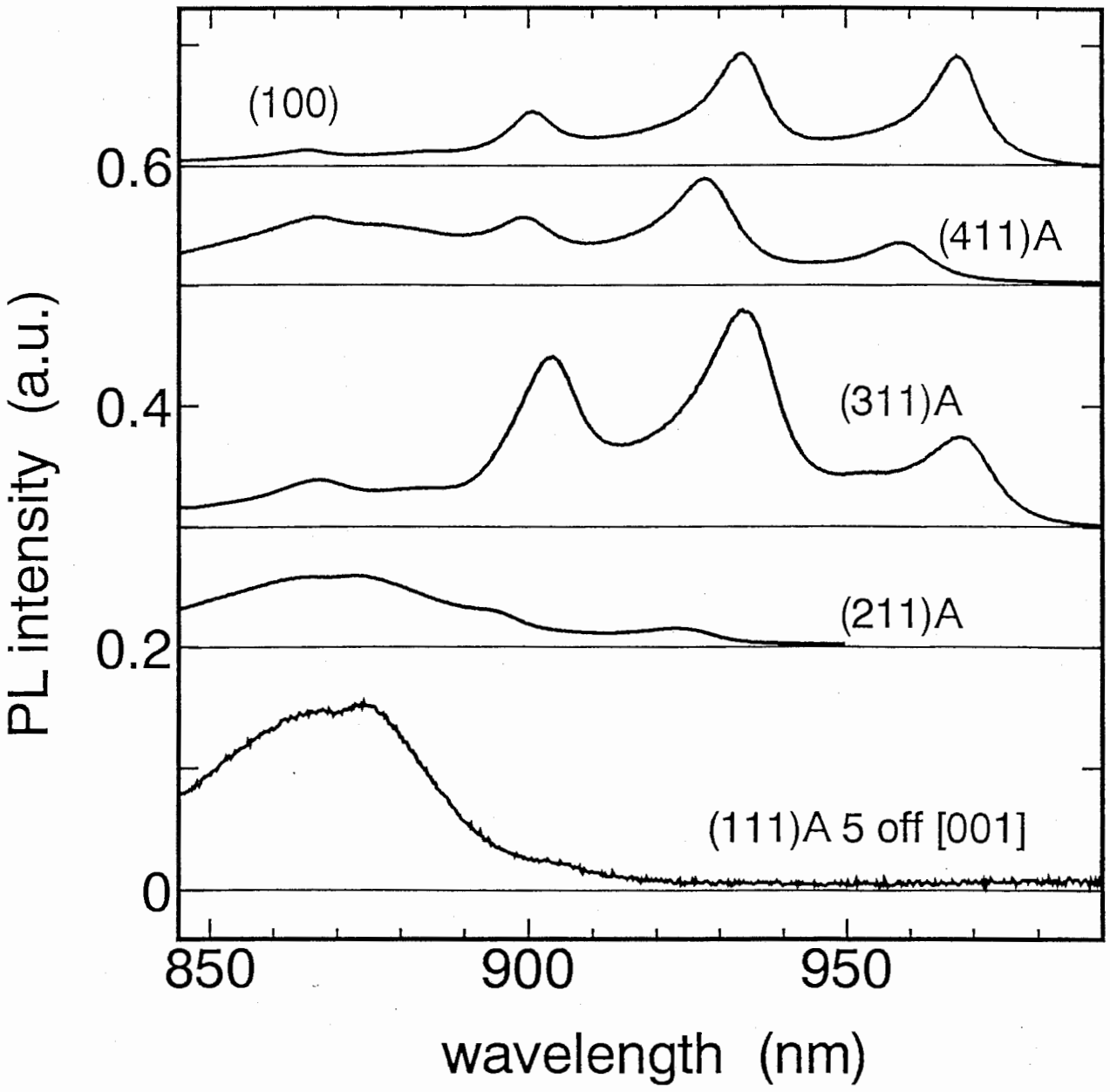

Figure 2.9: Photoluminescence spectra of samples with AlGaAs barriers for carrier confinement measured at 300K. The 1.43 eV peak is from the GaAs cladding layers. The spectra are shifted vertically for clarity. Excitation: 844 nm, 100 mW.

Chapter III

Piezoelectric effect in a (311)A–oriented quantum well

3.1. Quantum wells on GaAs (311)A

The built–in electric field for SQWs grown on (311)–oriented substrates is expected to be one third of the field found in (111)–oriented samples.[1] However this field is strong enough to produce drastical changes in the energy levels and optical properties. Moreover, crystal quality and heterointerfaces which are even better than the ones achieved on (100)–oriented substrates can be obtained routinely on (311)A–oriented substrates.

$In_{0.2}Ga_{0.8}As$/GaAs SQWs were grown on semi–insulating (311)A–oriented and for comparison on (100)–oriented GaAs substrates. Growth conditions are the same as described in Chapter II.

Photoluminescence (PL) and photoluminescence excitation (PLE) measurements were performed at 12K using a tunable Ti–sapphire laser excited with an Ar^+ laser, a monochromator and InGaAs photomultiplier detector. The excitation intensity was adjusted using neutral density filters. Scanning electron microscope (SEM) observation at x10000 magnification of the grown epilayer showed only featureless, smooth surfaces.

3.2. Theoretical results

The built–in electric field in the InGaAs layers produces a difference of the chemical potential between the GaAs barriers, which is equilibrated by a charge transfer in a very similar way as in a p–n junction. This charge transfer decreases the electric field in the well and creates an electric field in the barriers with sign opposite to the field in the well. Since the structure is undoped we assume that the barriers are depleted of carriers and that the electric field is constant in the barriers. Therefore, the tilted barrier contributes to the carrier confinement as shown in Fig. 3.1.

The InGaAs layers are biaxially compressed in the plane of the SQWs. This strain increases the bandgap and shifts the band alignment at heterointerfaces. The strained bandgap, band alignment, energy levels and wave functions were calculated as descibed in Chapter II. Parameters used in the calculation are shown in Table I. The values for InGaAs were obtained using linear interpolation. The elastic constants are taken from ref. 1 and the effective masses for (311)A–oriented GaAs are taken from ref. 3. We used the same effective masses for InAs because these values are not available. The (311)–oriented 10 nm SQW

without piezoelectric field has only two bound levels for electrons and four for heavy holes. The light holes band becomes type–II accordingly to our calculation. However, when the piezoelectric field is included several new bound levels appear in the electron and heavy hole bands. Figure 3.1 also shows the carrier probability density, i.e., the squared modulus of the wave function, for the lower levels of the electron and hole bands. The wave function for the first level of electrons is confined in the well but the wave function for the second level is located mainly in the tilted barrier. Higher levels are even more spread into the barrier. On the other hand, the wave functions for holes remain confined in the well up to the third level. From the overlap of the wave functions we can expect strong transition probabilities between the first level for electrons and various heavy hole levels. In addition, the light holes also become confined between the edge of the well and the tilted GaAs barrier. The first and second light hole levels have a considerable wave function overlap with the first electron level and we also expect strong transition probabilities. The Coulomb term of the Hamiltonian was neglected in this calculation but it would increase the overlap of the wave functions if included.[2)]

3.3. Identification of the energy levels

The well's composition was obtained by fitting the PLE spectrum of (100)–oriented samples with calculated values (see Fig. 3.2). This fitting method is valid as long as InGaAs growth rate and composition are independent of well thickness and accurate band parameters are available. An indium content of x=0.188 gave the best fit for the three wells. We will discuss in detail the 10 nm SQW because it has the largest quantity of bound levels. Figure 3.2 shows the PLE and PL spectrum for the 10 nm SQW grown on a (100)–oriented substrate. The full–width at half–maximum (FWHM) of the PL peak is 6 meV and the Stokes shift is 3 meV. The heavy hole exciton binding energy was estimated to be about 8 meV from the separation of the shoulder in the (1,1)H peak's high–energy side. The light hole exciton binding energy was calculated to be about 10 meV using the ratio between heavy and light holes exciton binding energies for GaAs/AlGaAs SQWs.[4)]

Figure 3.3 shows the PLE and PL spectrum for a 10 nm SQW grown on (311)A–oriented substrate. The quality of the sample is as good as or better than the (100) one as it can be appreciated from the FWHM of the (1,1)H peak. Furthermore the PL peak is about three times more intense and the Stokes shift is only 2 meV. The peaks' position does not change when detection wavelength is changed. This is a confirmation that these peaks are not phonon replicas. The transition energies were calculated using the composition and exciton binding energies obtained from the (100)–oriented sample. It has been shown that exciton

binding energies are rather insensitive to the crystal orientation.[4] The calculated values without and with piezoelectric field are shown above the spectrum. The upper row shows transition energies without piezoelectric field. The electron–heavy hole transitions without piezoelectric field do not coincide with the experimental spectrum. The light hole band has not bound levels because the alignment is type–II. The transition between the electron fundamental level and the light hole band edge is indicated as (1,n)L in Fig. 3.3.

On the other hand, the values calculated including the piezoelectric effect agree with the experimental results. We calculated the strain generated electric field from bulk piezoelectric theory.[1] For x=0.188 on the (311) direction, the theoretical electric field is E=80 kV/cm. The lower row shows the transition energies calculated using this field. Because the SQW's potential profile is not symmetric, transitions that were forbidden in the absence of an electric field now are allowed. Accordingly to the overlap of the wave functions, the heavy holes transitions (1,n)H with n=1,2,3 will be strong. Light holes transitions (1,n)L with n=1,2 also have some overlap. On the other hand, transitions involving excited electron levels are expected to be very weak. In addition, the (1,1)H transition is expected to be redshifted about 18 meV due to the electric field.

We identified tentatively the PLE spectrum peaks by comparison with the calculated transition energies. Transitions (1,1)H, (1,2)H and (1,3)H are clearly observable. Transition (1,4)H is superposed on transition (1,1)L then only one peak can be seen. Superposed with transition (1,2)L is transition (1,6)H (not drawn) flanked by transition (1,5)H. All these transitions would appear as the broader peak at 1.412 eV. Small shoulders associated to higher transitions are also visible.

The many peaks that appear superposed from 1.4 eV are related to the emergence of new hole energy levels confined between the SQW and the tilted barrier. The slope of this barrier can be tailored by changing its thickness and by adjusting the well thickness and composition.

The agreement between calculated values and measured values is remarkable. However, a small difference of 4 meV between the calculated energy for the SQW's (1,1)H transition and the value measured by PLE is observed. This difference as well as the difference between calculated and measured values in other transitions can be originated from many factors. The following is a discussion about the relative importance of some of these factors.

3.4. Other effects affecting the PLE spectrum

We observed about 1 meV redshift of the PL peak shown in Fig. 3.3 when decreasing the excitation intensity to obtain the minimum detectable PL spectrum. Moreover, the electric field screening due to photogenerated carrier is less

than 0.3 kV/cm under our experimental conditions (excitation intensity about 14 W/cm^2). Thus, screening due to photogenerated carriers is not the origin of the observed difference.

Other possibility for this difference is the reduction of the exciton binding energy due to the electric field. Bastard[4] calculated a binding energy reduction of about 1 meV for a 10 nm thick AlGaAs/GaAs QW with 70 kV/cm applied electric field. Since barrier height is smaller in InGaAs/GaAs, a larger energy reduction can be expected.

A surface charge density at the heterointerfaces of about $7x10^{-5} C/m^2$ could be also an explanation of this difference. Charge trapped at heterointerface defects produces an electric field opposite to the piezoelectric field that reduces the band tilt in the well and blueshifts the transition energies. R.L. Tober et al.[5] made samples with AlGaAs barriers and A. Pabla et al.[6] used GaAs barriers. Both groups used (111)B-oriented GaAs substrates and indium composition x=0.15. They measured electric fields 30% smaller than the theoretical values and suggested that a surface charge as large as $7x10^{-4}$ C/m^2 could be present at the heterointerfaces. Our samples would have a smaller surface charge as compared with samples grown on (111)B substrates.[5]

So far, we implicitly assumed that the InGaAs growth rate and composition are the same on (100) and (311)A-oriented surfaces; but it is not necessarily true. A 10% faster growth rate on the (311)A-oriented surface is enough for obtaining the 4 meV shift observed.

3.5. Conclusions

In conclusion, high quality InGaAs/GaAs SQWs were grown on (311)A-oriented substrates. The built-in electric field generated in the strained layer by piezoelectric effect was studied using PL and PLE spectroscopy. The PLE spectrum shows large changes in the energy levels. The most notable features are strong peaks related with transitions forbidden in the absence of electric field and the emergence of new energy levels confined by the tilted barrier in the holes bands. The observed features agree with the presence of a piezoelectric field of about 80 kV/cm. Because the wider range of growth conditions that give high quality SQWs, (311)A-oriented substrates come forth as an alternative for making structures that take advantage of the piezoelectric effect.

References to chapter III

1) D. Sun and E. Towe: Jpn. J. Appl. Phys. **33** (1994) 702.
2) P. Debernardi and P. Fasano: IEEE J. Quantum Electron. **29** (1993) 2741.

3) O. Brandt, K. Kanamoto, Y. Tokuda, N. Tsukada, O. Wada and J. Tanimura: Phys. Rev. **B48** (1993) 17599.
4) G. Bastard: *Wave Mechanics Applied to Semiconductor Heterostructures* (Halsted Press, New York, 1988) Chap. 8, p. 303.
5) R. L. Tober and T. B. Bahder: Appl. Phys. Lett. **63** (1993) 2369.
6) A. Pabla, J. Sanchez–Rojas, J. Woodhead, R. Grey, J. David, G. Rees, G. Hill, M. A. Pate, P. Robson, R. Hogg, T. Fisher, A. Willcox, D. Whittaker and M. Skolnick: Appl. Phys. Lett. **63** (1993) 752.

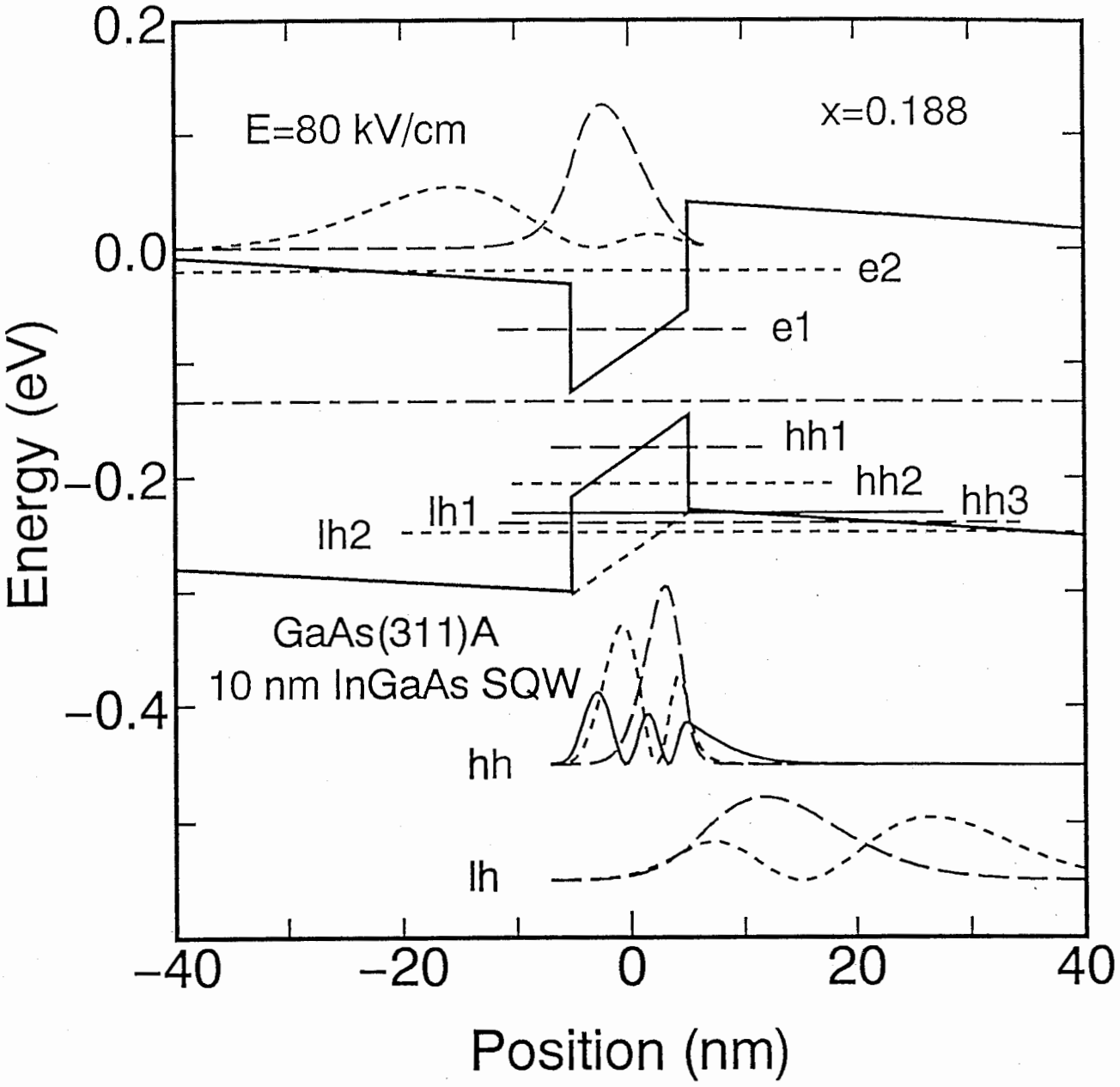

Figure 3.1: Potential profile of electron and hole bands. The light hole band that is split from the heavy holes band in the well is drawn with short dashes between the edges of the well. Electron (e), heavy hole (hh) and light holes (lh) energy levels and wave functions are also drawn. First, second and third levels are indicated as long dashed, short dashed and full lines respectively.

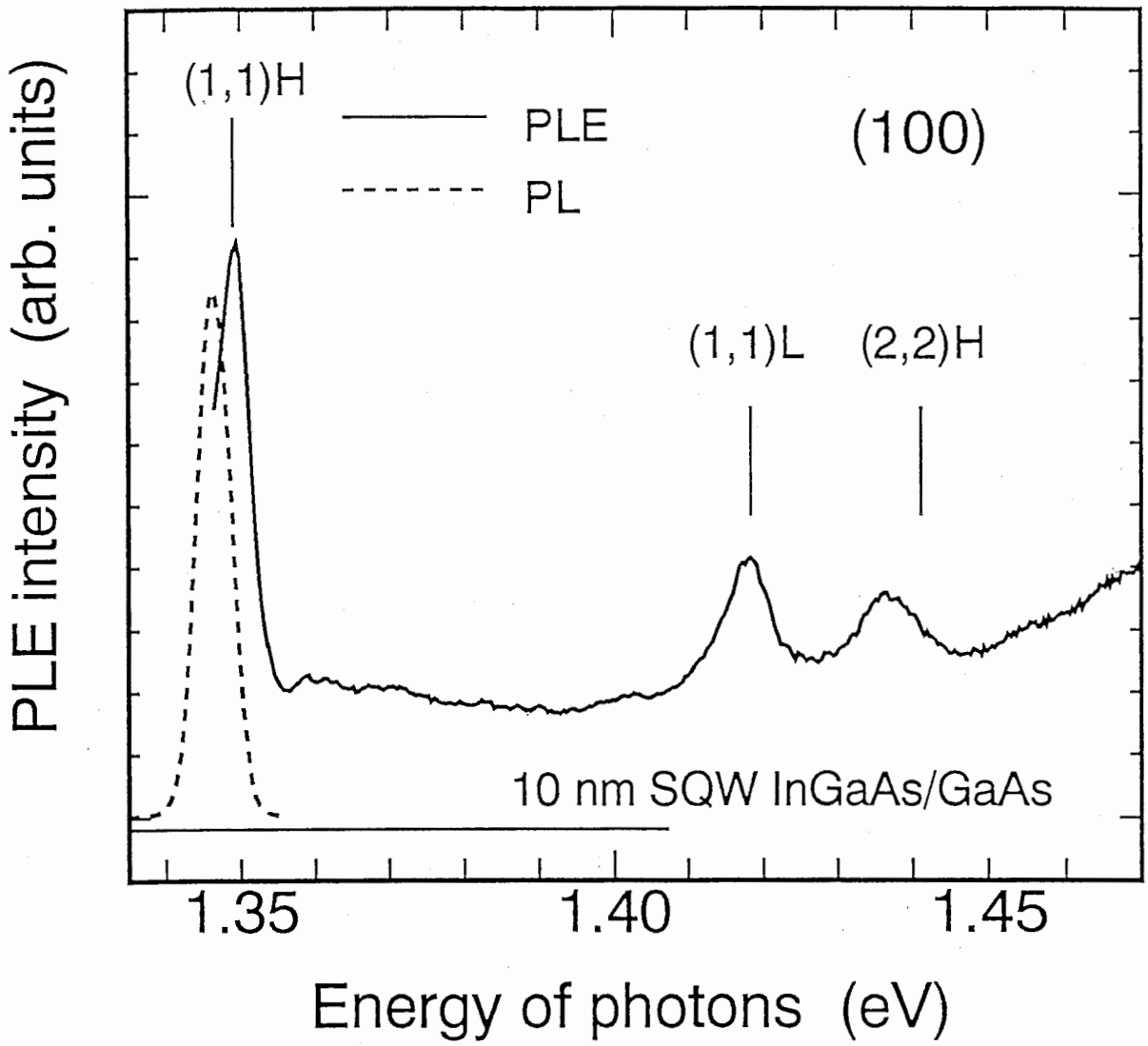

Figure 3.2: Photoluminescence and PLE spectrum of a 10 nm SQW grown on a (100)–oriented substrate. Vertical bars indicate the calculated transition energies for an indium content of x=0.188.

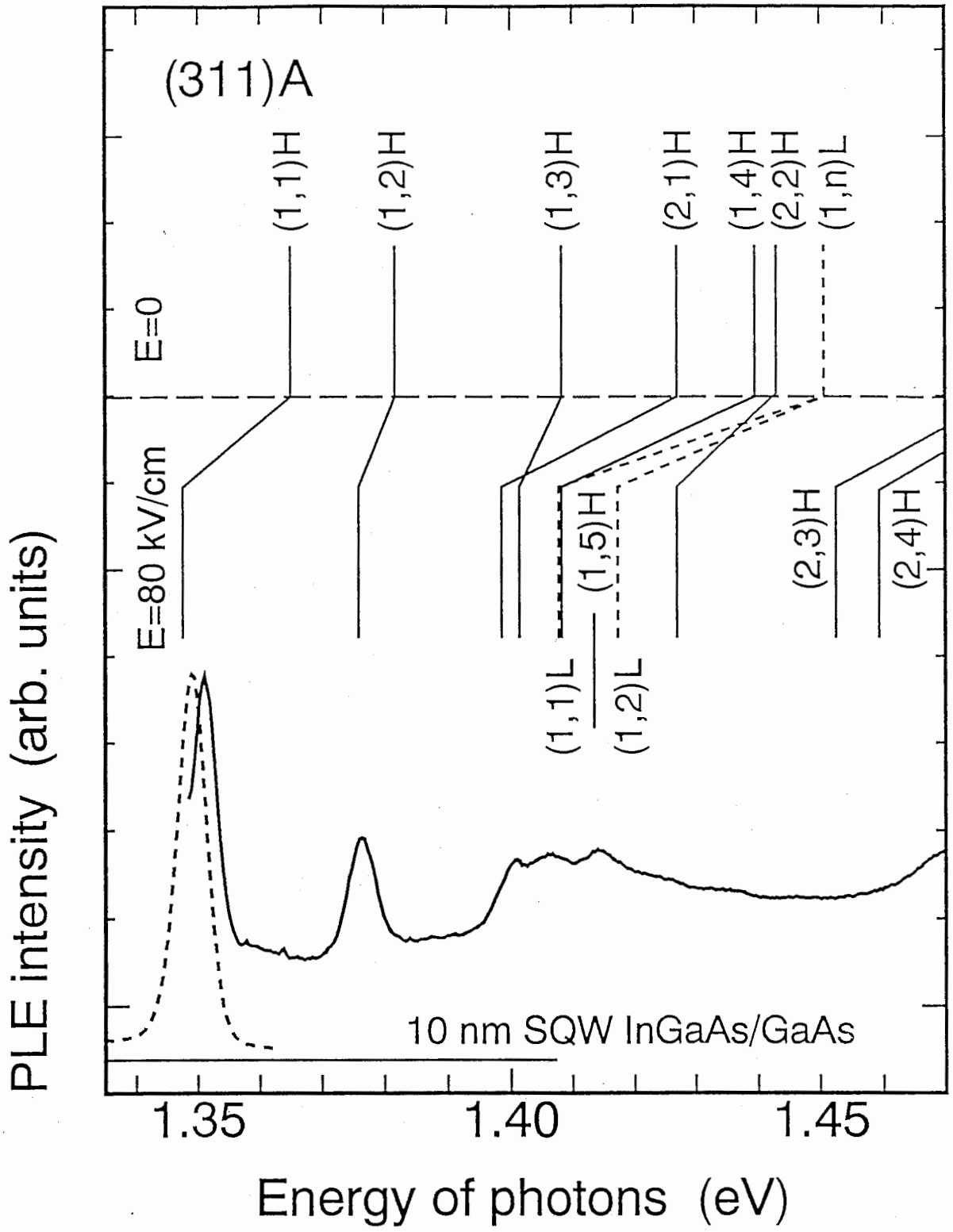

Figure 3.3: Photoluminescence (dashed line) and PLE (full line) spectrum of a 10 nm SQW grown on a (311)A–oriented substrate. Vertical bars indicate the calculated transition energies for an indium content of x=0.188. The upper row shows transition energies calculated without electric fields in the structure. The lower row shows transition energies calculated including the 80 kv/cm electric field produced by the piezoelectric effect. Full–line bars are heavy holes transitions and dashed–line bars are light holes transitions.

Chapter IV

Control of the energy levels using an applied voltage

4.1. Blueshift of the optical transition energies

The piezoelectric field in InGaAs/GaAs strained quantum wells (SQW) grown on GaAs (111) substrates redshifts the optical transition energies accordingly to the quantum confined Stark effect (QCSE). If an external electric field opposite to the built–in electric field is applied, a blueshift of the optical transition energies can be observed.[1] This blueshift has been observed by photocurrent spectroscopy and electroreflectance spectroscopy in SQWs embedded in the insulating region of *p–i–n* diodes.[2,3] All but a few of these structures have been grown on (111)B–oriented substrates because they provide the largest built–in electric field. The (111)A–oriented substrates provide the same built–in electric field but crystal growth is by far more difficult.[4] The electric field in SQWs grown on gallium terminated (A) substrates has the opposite direction of the electric field in SQWs grown on arsenic terminated (B) substrates. This property can be desirable when designing some devices.

In this chapter, we report the first observation of blueshift of the optical transition energies by photoluminescence spectroscopy in $In_{0.2}Ga_{0.8}As$/GaAs SQWs grown on (111)A GaAs.

4.2. Structure of the *p–i–n* diodes

As described in Chapter II, the SQWs grown on GaAs (111)A 5° off toward [001]–oriented substrates showed the best optical characteristics, thus, this substrate orientation was chosen for growing samples on p–doped substrates and making *p–i–n* diodes.

Growth conditions are the same of Chapter II. The As_4 beam equivalent pressure was $2.2x10^{-5}$ Torr and the As_4/Ga flux ratio was 6.5. This high As_4/Ga flux ratio has two purposes. Firstly, it is required to obtain smooth surfaces on (111)A–oriented samples. Secondly, it assures that the amphoterous dopant silicon is incorporated as a donor. The *p–i–n* diode structure consisted of 120 nm Be–doped ($2x10^{18}cm^{-3}$) GaAs buffer layer, 80 nm nonintentionally doped (NID) GaAs spacer, 10 nm NID $In_{0.2}Ga_{0.8}As$ SQW, 80 nm NID GaAs spacer, 5 nm NID $In_{0.2}Ga_{0.8}As$ SQW, 80 nm NID GaAs spacer, 2.5 nm NID $In_{0.2}Ga_{0.8}As$ SQW, 80 nm NID GaAs spacer, and 120 nm Si–doped ($2x10^{18}cm^{-3}$) cap layer. This structure is shown in Fig. 4.1. The doped samples were processed into mesa diodes, as shown in Fig 4.1. Au/Ni/AuGe and Au contacts were evaporated on

the n–side and p–side, respectively, and annealed 2 min at 350°C. The top contact (n–side) was patterned in 0.4 mm squares with a 0.2 mm circular window for optical access. Square mesas with 0.4 mm sides were made using wet etching.

4.3. Photoluminescence spectrum dependence on voltage bias

Figure 4.2 shows the potential profile of the electron and hole bands calculated for the 10 nm SQW. The band edge tilt due to the built–in electric field is so strong that both electrons and holes are confined in triangular quantum wells. A smaller value of electric field is used in Fig. 4.2 to fit experimental data, as is explained below. The electrons' confinement in the wells is improved by the tilted GaAs barrier.

Figure 4.3 shows the PL spectra of the diodes with applied bias. Low excitation intensity (less than 1 W/cm^2) was used to avoid screening the electric field with photogenerated carriers. The PL peak corresponding to the 10 nm SQW blueshifted as much as 24 meV with only 1.2 V applied reverse bias. At this point it becomes clear that the piezoelectric field in our samples grown on (111)A substrates has the opposite direction of samples grown on (111)B substrates. Our samples grown on p–type (111)A substrates show a blueshift with reverse applied bias. On the other hand, n–type (111)B substrates have to be used to obtain a blueshift with reverse applied bias.[3)] The larger FWHM of the PL peaks, as compared to the undoped samples, can originate in the annular contact that produces an inhomogeneous electric field in the SQWs. Figure 4.4 shows the PL peak dependence on applied electric field. The dotted lines are calculated using a piezoelectric field value 24% smaller than the calculated value. The agreement between calculated and experimental values is only qualitative. The discrepancy can be related to the inhomogeneous electric field applied to the quantum wells. The applied electric field becomes inhomogeneous because of the large window area and low donor concentration in the cap layer. Donor concentration is low because Si occupies many acceptor sites on GaAs (111)A 5° off toward [001]–oriented substrates even under the high As_4 pressure used during MBE growth. The blueshift is nearly linear with applied reverse bias because more than 6 V are required to reach the flat band condition in the SQW.

The discrepancy between theory and the piezoelectric fields of the undoped samples can be related to the presence of surface charge at the heterointerfaces. A surface charge density of 9×10^{-8} C/cm^2 will cause the observed reduction in the built–in electric field.

We have grown the InGaAs layers used in this work at a quite high temperature because we wanted strong PL. However, the high growth temperature also promotes strain relaxation and the consequent reduction of the piezoelectric field. It is better to grow the InGaAs layers at lower temperatures for devices based on

excitonic absorption.

The large blueshift of the PL peak energy under moderated illumination intensity suggests the possibility of application for optical bistable devices.[5] These devices need an external bias when they are grown on GaAs (100) substrates to obtain a redshift of the excitonic absortion peak. We propose a charge-induced self-feedback device (CSFD) which does not require an external applied bias to operate. In the CSFD device, the feedback is due to field-screening, allowing the independent switching of optical beams focused at different spots on the CSFD without the need of pixellation. The originality of our design consists of taking advantage of the piezoelectric field generated inside InGaAs strained quantum wells (QWs) grown on GaAs (111) oriented substrates. Thus the device is an as-grown undoped structure without electrical contacts.

Figure 4.5 shows the device structure and operation principle. The active region consists of an $In_{0.05}Ga_{0.95}As$ multiple quantum well (MQW) structure with $Al_{0.2}Ga_{0.8}As$ barriers. This region is bounded by higher $Al_{0.5}Ga_{0.5}As$ barriers to confine photocarriers. In the absence of optical excitation (Fig. 4.5 (a)), the InGaAs QWs are tilted due to the built-in piezoelectric field. This field redshift the exciton absorption peak accordingly to the quantum-confined Stark effect (QCSE). By illuminating the device by an optical beam with wavelength a little shorter than the redshifted exciton peak, the photogenerated electrons and holes travel in opposite directions through the MQW and accumulate at the edges, screening the piezoelectric field as shown in Fig. 4.5 (b). This screening reduces the redshift of the absorption peak that moves nearer to the excitation beam wavelength and optical absorption increases. The increased absortion generates more photocarriers and the positive self-feedback is established. Figure 4.6 shows the expected bistable behaviour of this device.

4.4. Conclusions

InGaAs/GaAs SQWs grown on GaAs (111)A 5° off toward [001]-oriented substrates were embedded in the *i*-region of *p-i-n* diodes. The PL spectrum shows the influence of a built-in electric field due to the piezoelectric effect. The blueshift of PL peaks with applied reverse bias was demonstrated in a *p-i-n* structure. We also demonstrated that the direction of the piezoelectric field on (111)A-oriented samples is opposite to that of (111)B-oriented samples. The large blueshift and good optical properties observed are promising for the integration of optical modulators with other devices on (111)A GaAs.

References to chapter IV

1) C. Mailhiot and D. Smith: Phys. Rev. **B35** (1987) 1242.
2) R. Tober and T. Bahder: Appl. Phys. Lett. **63** (1993) 2369.
3) A. Pabla, J. Sanchez–Rojas: J. Woodhead, R. Grey, J. David, G. Rees, G. Hill, M. Pate, P. Robson, R. Hogg, T. Fisher, A. Willcox, D. Whittaker and M. Skolnick, Appl. Phys. Lett. **63** (1993) 752.
4) T. Yamamoto, M. Inai, T. Takebe and T. Watanabe: J. Vac. Sci. Technol. 11 (1993) 631.
5) G. Hayashi, S. Kodama, Y. Yamaoka, A. Takano, K. Hirakimoto, Y. Lee and M. Yamanishi: IEEE J. Quantum Electron. **29** (1993) 2655.

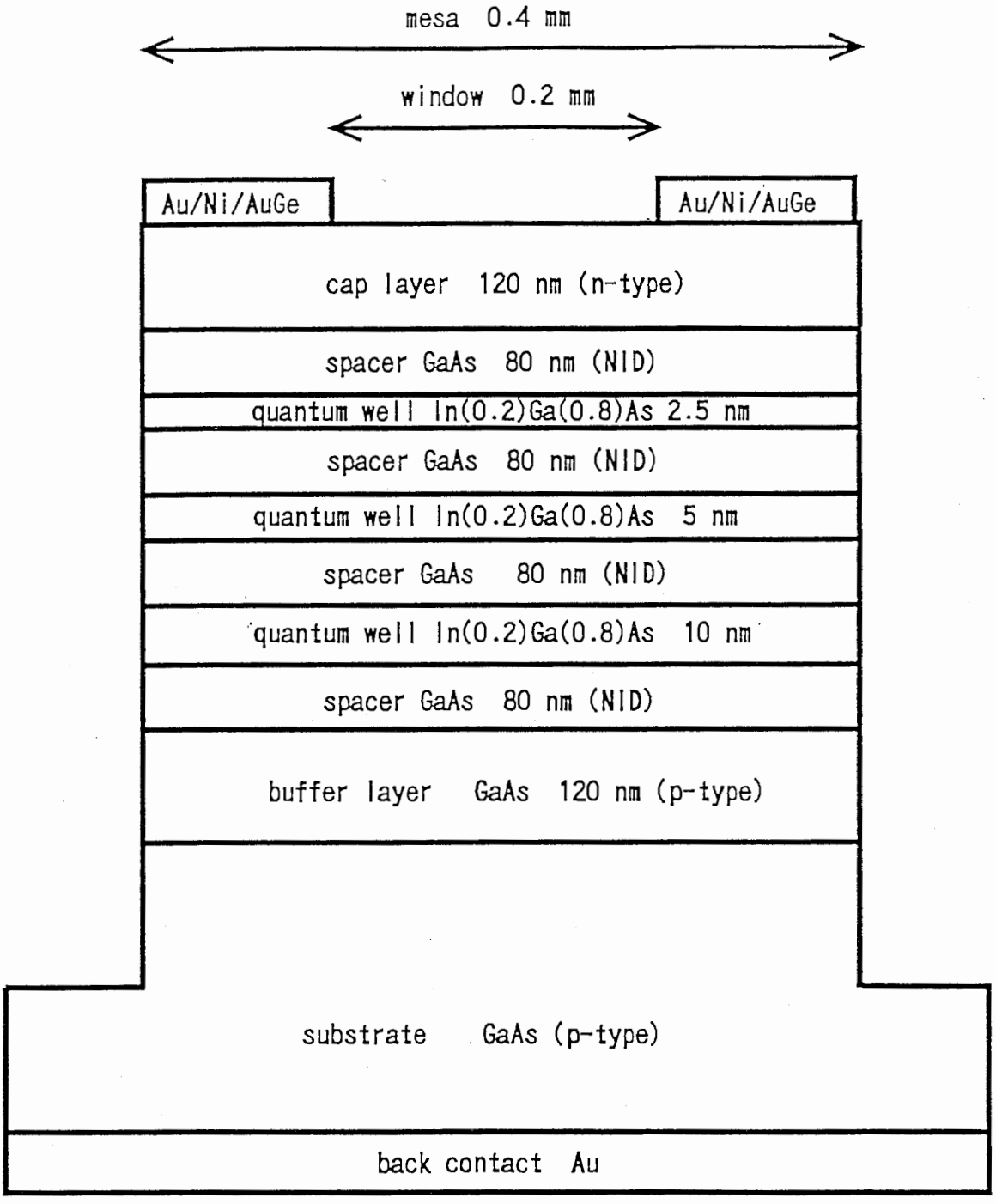

Figure 4.1: Structure of the p–i–n diodes. The undoped samples have the same multilayer structure.

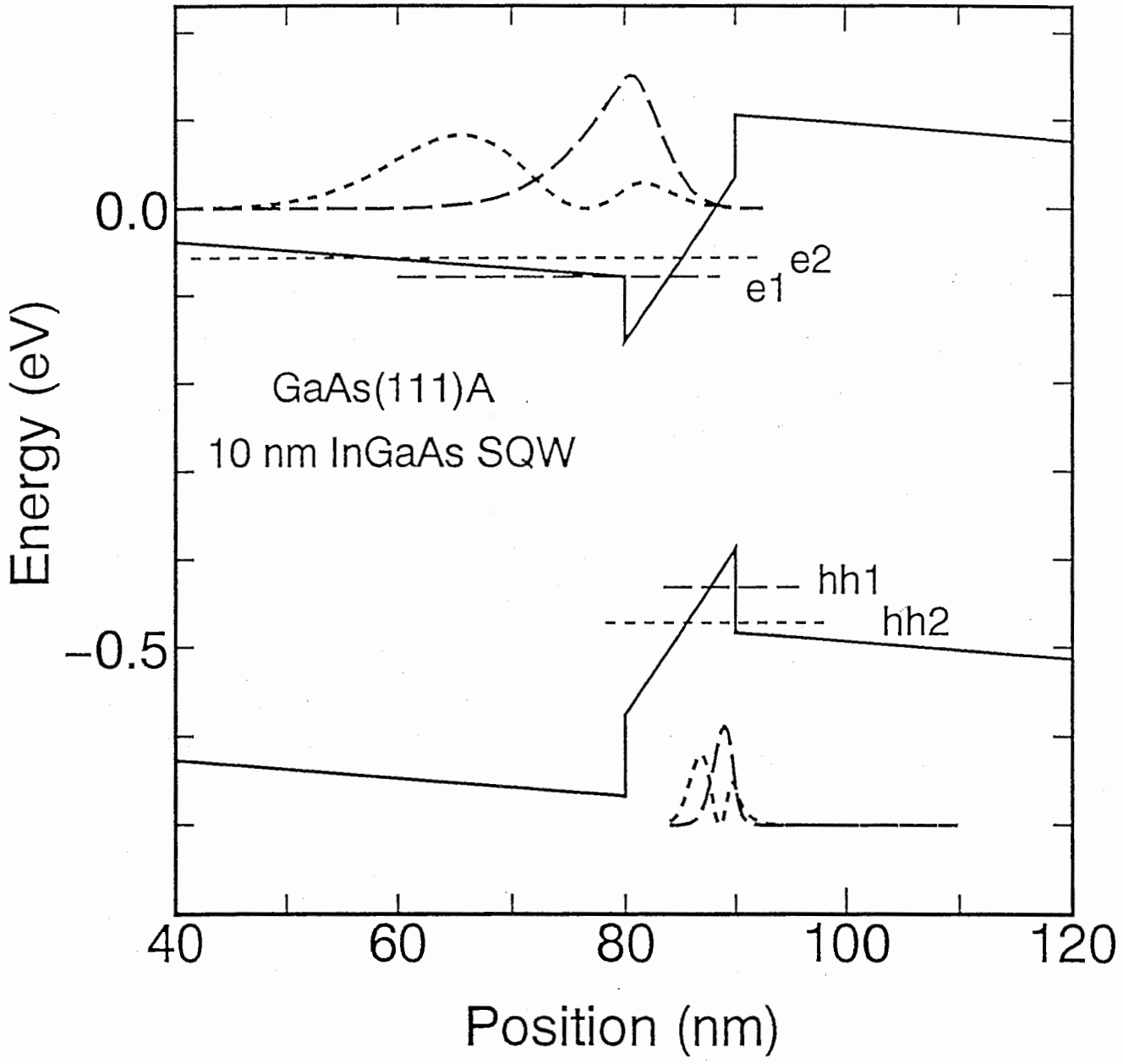

Figure 4.2: Potential profile for the 10 nm SQW. The two lower energy levels for electrons and holes, and their wave functions are shown. The built–in electric field in the barrier helps to confine the electrons in the well. The band gap is not at scale with the potential profile of the band edges.

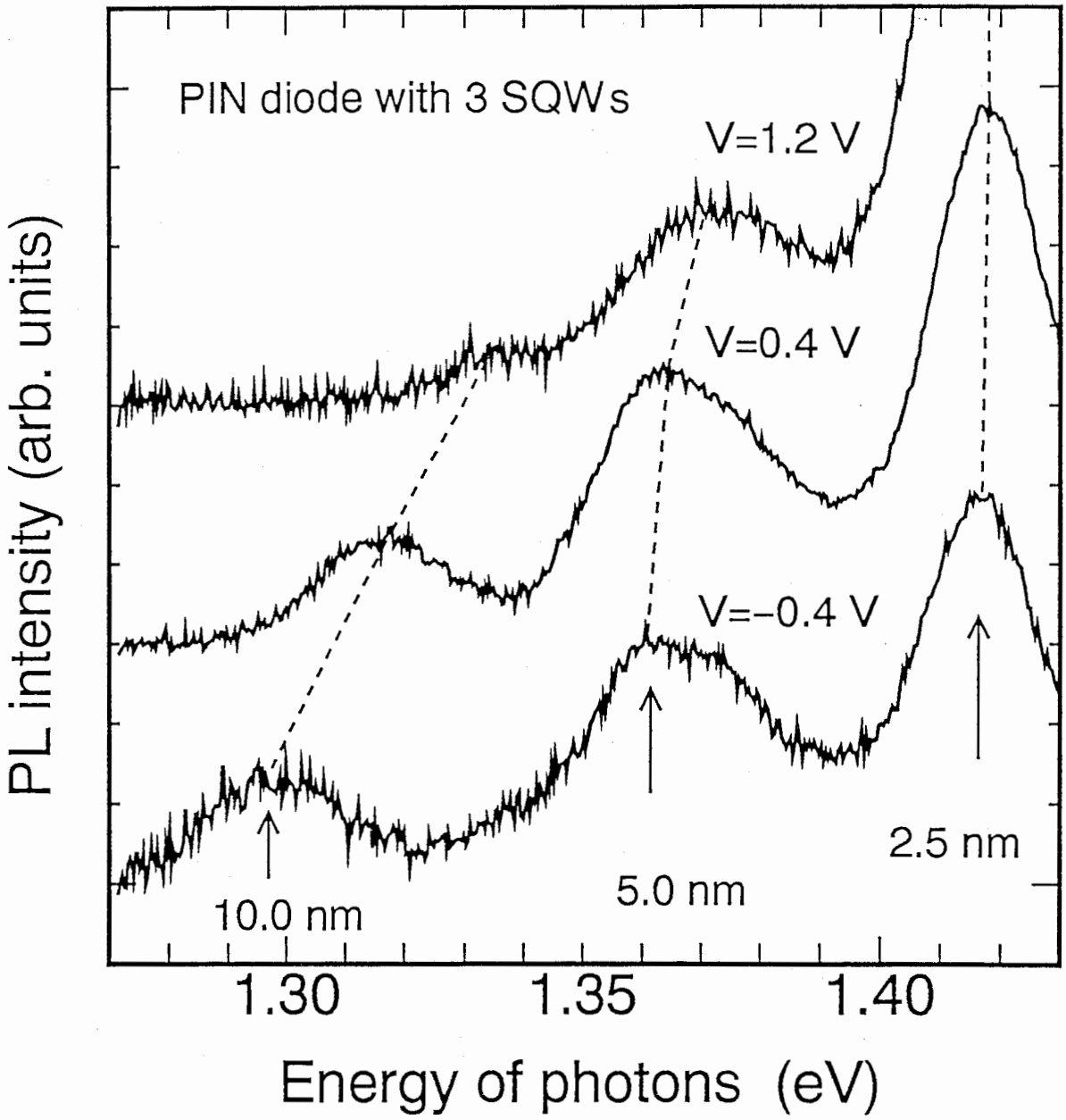

Figure 4.3: Photoluminescence spectra of a $p-i-n$ diode. The PL peak shifts toward higher energy as reverse bias is increased.

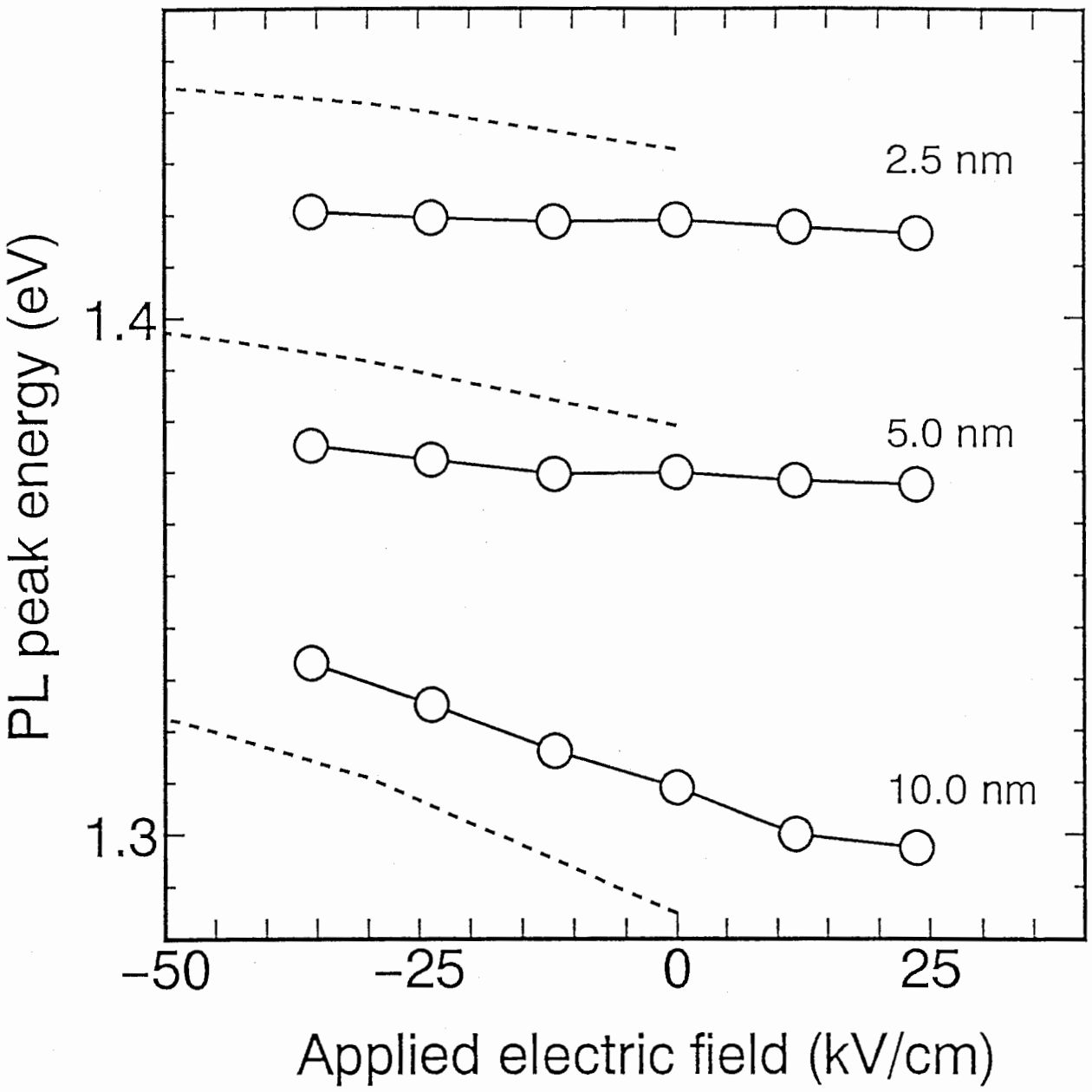

Figure 4.4: Photoluminescence peak energy dependence on applied electric field. The dotted line is the calculated value for a piezoelectric field of 196 kV/cm.

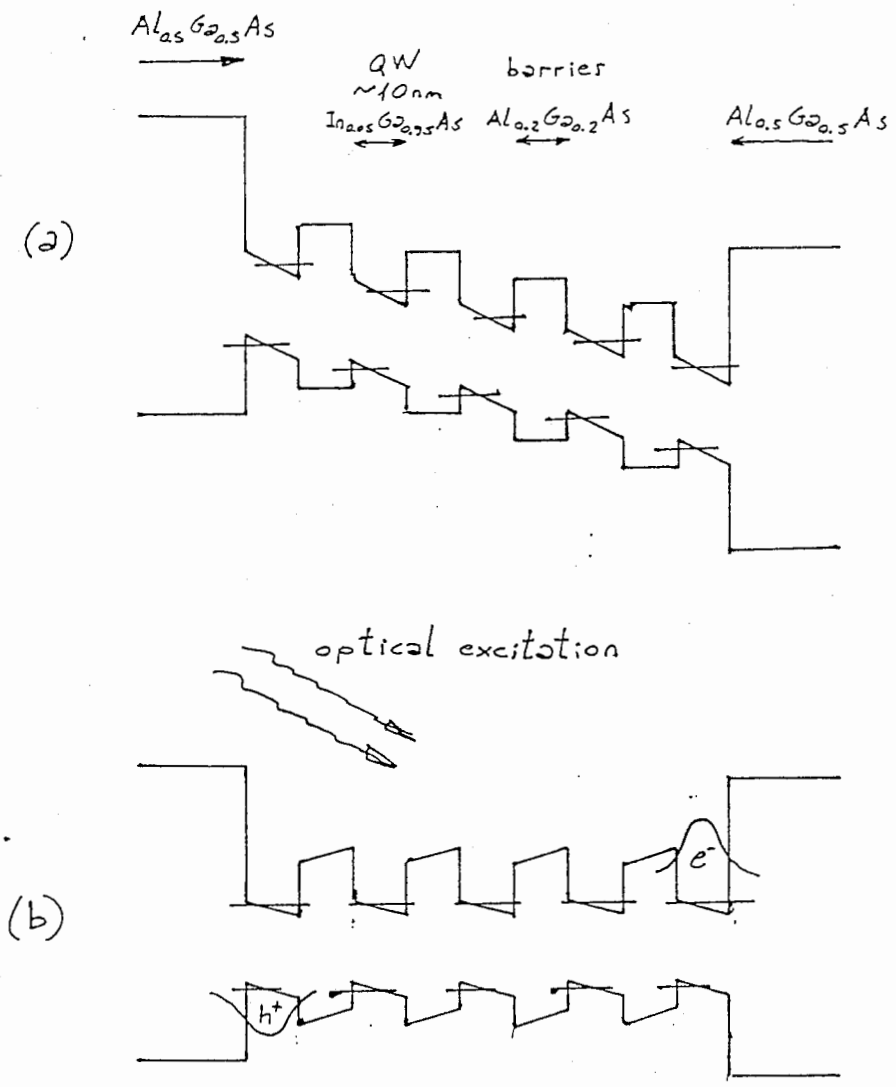

Fig. 1

Figure 4.5: Charge–induced self–feedback device which has a built–in electric field due to piezoelectric effect. (a) Without optical excitation the absorption peak is redshifted due to the quantum–confined Stark effect. (b) Under optical excitation the redshift is reduced due to screening of the piezoelectric field by photogenerated carriers.

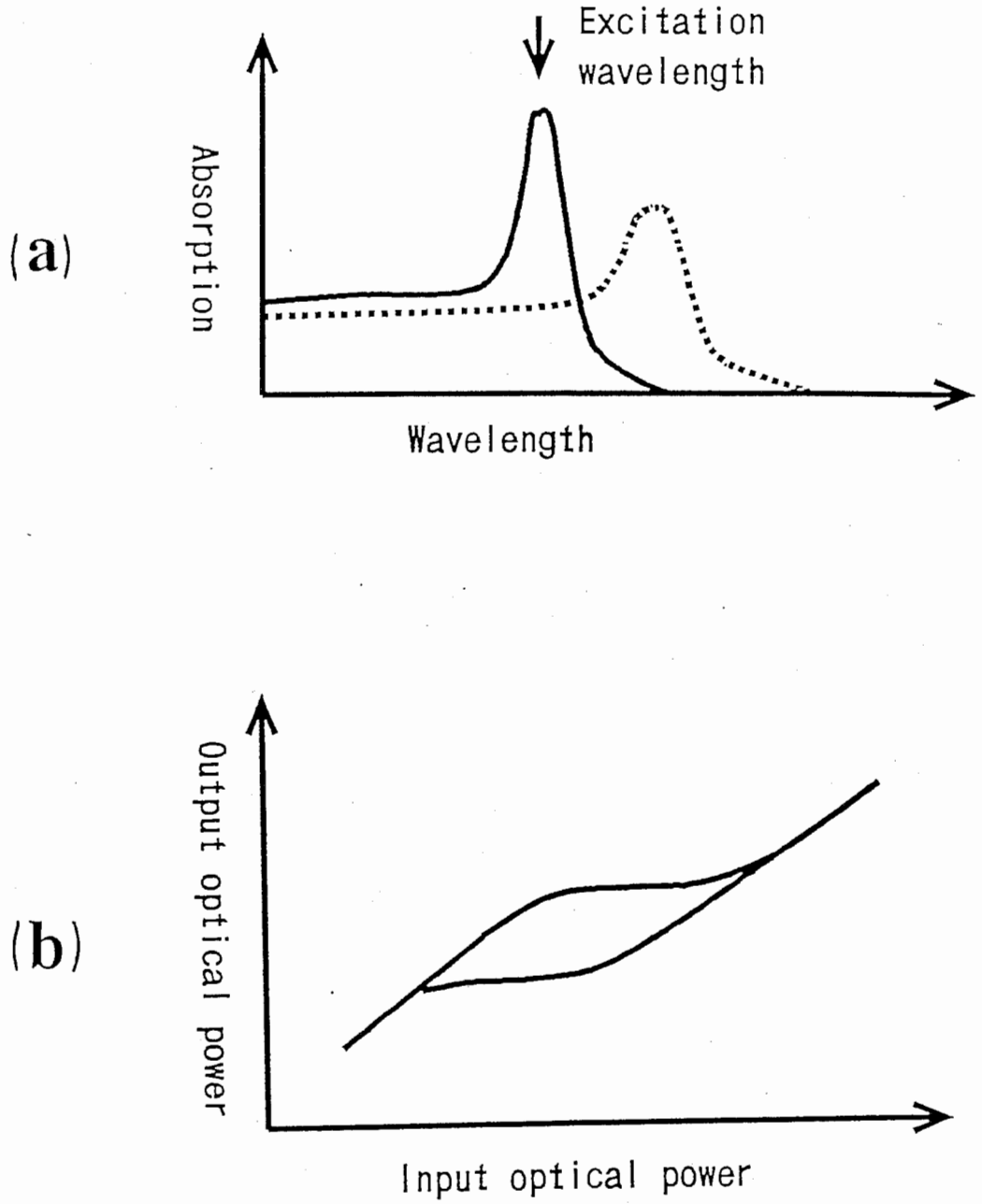

Figure 4.6: Bistable behavior of the charge–induced self–feedback device. (a) The device is excited at a wavelength shorter than the exciton peak. The exciton peak moves toward shorter wavelength as the photogenerated carriers screen the piezoelectric field. Absorption increases non–linearly when the exciton peak reaches the excitation wavelength. (b) The non–linear optical absorption increase with optical excitation produces bistability.

Chapter V

Influence of the piezoelectric effect on the carrier dynamics

5.1. Optical nonlinearities

Strained quantum well (QW) structures of InGaAs/GaAs grown on GaAs (111)A–oriented substrates have a built–in electric field due to piezoelectric effect as described in the previous chapter.

Optical nonlinearities are observed in these structures when the electric field is screened by photogenerated carriers. The carrier dynamics of the electric field screening has been studied in multiple QW structures measuring the absorption coefficient dependence on carrier density.[1,2] These experiments show that the electric field screening is mainly due to carriers that escaped from the wells and screen the entire multiple QW structure. The dynamics of the electric field screening inside each quantum well cannot be properly studied in these multiple QW structures.

In contrast to the above absorption experiments using multiple QW structures, in this paper we study the electric field screening dynamics in a *single* QW with piezoelectric effect using time–resolved photoluminescence (PL) spectroscopy. Unusual behavior of the PL intensity decay for different wavelengths is observed and explained clearly using a simple model.

An $In_{0.2}Ga_{0.8}As$/GaAs QW with a 10 nm thickness was grown on (111)A–oriented and for comparison on (100)–oriented GaAs substrates. Growth conditions and characterization are the same of Chapter II. The PL was excited using light pulses from a mode locked Ti:sapphire laser (757 nm wavelength, 100 fs pulse–width, 82 Mhz repetition rate) and it was measured using a streak camera. The experimental set–up is shown in Fig. 5.1. Measurements were performed at 20 K.

5.2. Photocarriers dynamics

After the optical excitation pulse, the PL peak position of the (111)A–oriented sample moves toward longer wavelength as the photogenerated carrier density in the well decreases with time, as shown in Fig. 5.2. On the other hand, the (100)–oriented sample does not show significant change of the PL peak position. The PL peak intensity of the (111)A–oriented sample shows a non–exponential dependence on time, as shown in Fig. 5.3. The (100)–oriented sample shows the usual mono–exponential decay attributable to excitonic recombination. The full

lines on the (111)A data in both figures are calculated accordingly to the following model. There is a photogenerated electron density n_0 and a hole density p_0 ($n_0 > p_0$) in the well just after the excitation pulse. The assumption that $n_0 > p_0$ can be justified considering that electrons generated between the well and the sample's front surface have more probability of being captured than holes because the direction of the piezoelectric field. Therefore, the PL intensity will depend on the hole density and the electric field screening will depend on the electron density. The rate equations for the carrier density, assuming excitonic recombination and neglecting non-radiative recombination, are:

$$\begin{cases} \frac{dn}{dt} = -\frac{P}{\tau_{rad}} \\ \frac{dp}{dt} = -\frac{P}{\tau_{rad}} \end{cases} \tag{5.1}$$

where the radiative recombination time constant τ_{rad} is a function of the electron and hole wave functions overlap M :

$$\tau_{rad} = \frac{\tau_0}{|M|^2} \tag{5.2}$$

In turn, the wave functions overlap depends on the total electric field in the well, that is the piezoelectric field screened by the photocarriers. We use the relationship between photocarrier density and electric field screening calculated by Rodríguez-Gironés and Rees.[3] We calculated the energy levels and wave functions overlap dependence on the electric field as described in Chapter II.

The PL intensity is given by:

$$I \propto \frac{P}{\tau_{rad}} \tag{5.3}$$

The rate equations are solved numerically. The n_0 value is obtained from the PL peak position just after the excitation pulse, the p_0 and τ_0 value are chosen to fit the experimental values of Figs. 5.2 and 5.3. The τ_0 value is approximately equal to the radiative recombination time constant that should be observed if the electric field were completely screened. It can be compared with a decay time constant of 0.6 nsec that we measured in samples with similar structure but grown on (100)-oriented substrates where there is not piezoelectric field. The shorter decay constant of the (111)A-oriented sample can be related to the higher optical transition rate in (111)-oriented QWs compared to (100)-oriented QWs.[4]

5.3. Wavelength-resolved PL decay time

Figure 5.4 shows the PL intensity decay curves measured at various wavelengths. The short wavelength curves (a), (b) show a fast initial decay followed by a slower decay. The long wavelength curves (c), (d) show an initial increases of the PL intensity followed by a slow decay. This unusual behavior is due to the carrier dynamics in the well. The high carrier density immediately after the excitation pulse screens the piezoelectric field. The electric field reduction in the well has two effects. First, the quantum-confined Stark shift decreases and the PL peak shift toward shorter wavelengths. Second, the electron and hole wave functions overlap increases and the oscillator strength for optical transitions also increases. The opposite effect occurs when the carrier density decreases by recombination. Therefore, the fast decay of PL intensity at short wavelengths is due to the combined effect of larger oscillator strength and shift of the PL peak toward longer wavelength. On the other hand, the PL intensity at longer wavelengths initially increases with time because the PL peak is redshifting; after this increase it decays slowly because the reduced oscillator strength.

We calculated the PL decay curves at various wavelengths using the model described above. The results shown in Fig. 5.5 were obtained assuming a Gaussian shape for the PL peak and using the FWHM experimental value of 27 meV. The other parameters are τ_o =0.3 ns, n_0=11.3x10^{11} cm^{-2} and p_0=9.0x10^{11} cm^{-2}. The shape of these curves is in qualitative agreement with the experimental results. Figure 5.6 show the PL time constant dependence on wavelength. Both, experimental and calculated values for the (111)A-oriented sample are obtained from the regions of maximum slope of the respective decay curves shown in Fig. 5.4 and 5.5. The PL time constants of (100)-oriented samples is shown for comparison. There is a fair agreement between experimental and calculated values. It indicates that our model succesfully includes the most relevant features of the experiment. Moreover, the few adjustable parameters have also physically reasonable values. We have grown the InGaAs layer at 560°C to obtain strong PL, but this relatively high growth temperature degrades the heteroface quality of the (111)A-oriented samples. Our samples have PL peaks with a large FWHM (27 meV) which obscures the increase of the PL intensity with time at long wavelengths (Fig. 5.4(d)).

5.4. Conclusions

In conclusion, we measured the time-resolved PL in $In_{0.2}Ga_{0.8}As/GaAs$ single quantum wells grown on (111)A-oriented substrates. The PL decay curves measured at various wavelengths show the carrier dynamics inside the well. The partial screening of the piezoelectric field by photogenerated carriers shifts the

PL peak to shorter wavelengths and increases the oscillator strength for optical transitions. The decrease of the photogenerated carriers by recombination gives unusual PL intensity decay curves. This effect is explained using a model that fits succesfully the experimental results.

References to chapter V

1) X. R. Huang, D. R. Harken, A. N. Cartwright, D. S. McCallum, A. L. Smirl, J. Sanchez–Rojas, A. Sacedon, F. Gonzalez–Sanz, E. Calleja, and E. Muñoz, J. Appl. Phys. **76**,7870 (1994).
2) D. R. Harken, X. R. Huang, D. S. McCallum, A. L. Smirl, J. Sanchez–Rojas, A. Sacedon, E. Calleja, and E. Muñoz, Appl. Phys. Lett. **66**,857 (1995).
3) P. J. Rodríguez–Gironés and G. J. Rees, IEEE Photon. Technol. Lett. **7**, 71 (1995).
4) T. Hayakawa, K. Takahashi, M. Kondo, T. Suyama, S. Yamamoto, and T. Hijikata, Phys. Rev. Lett. **60**, 349 (1988).

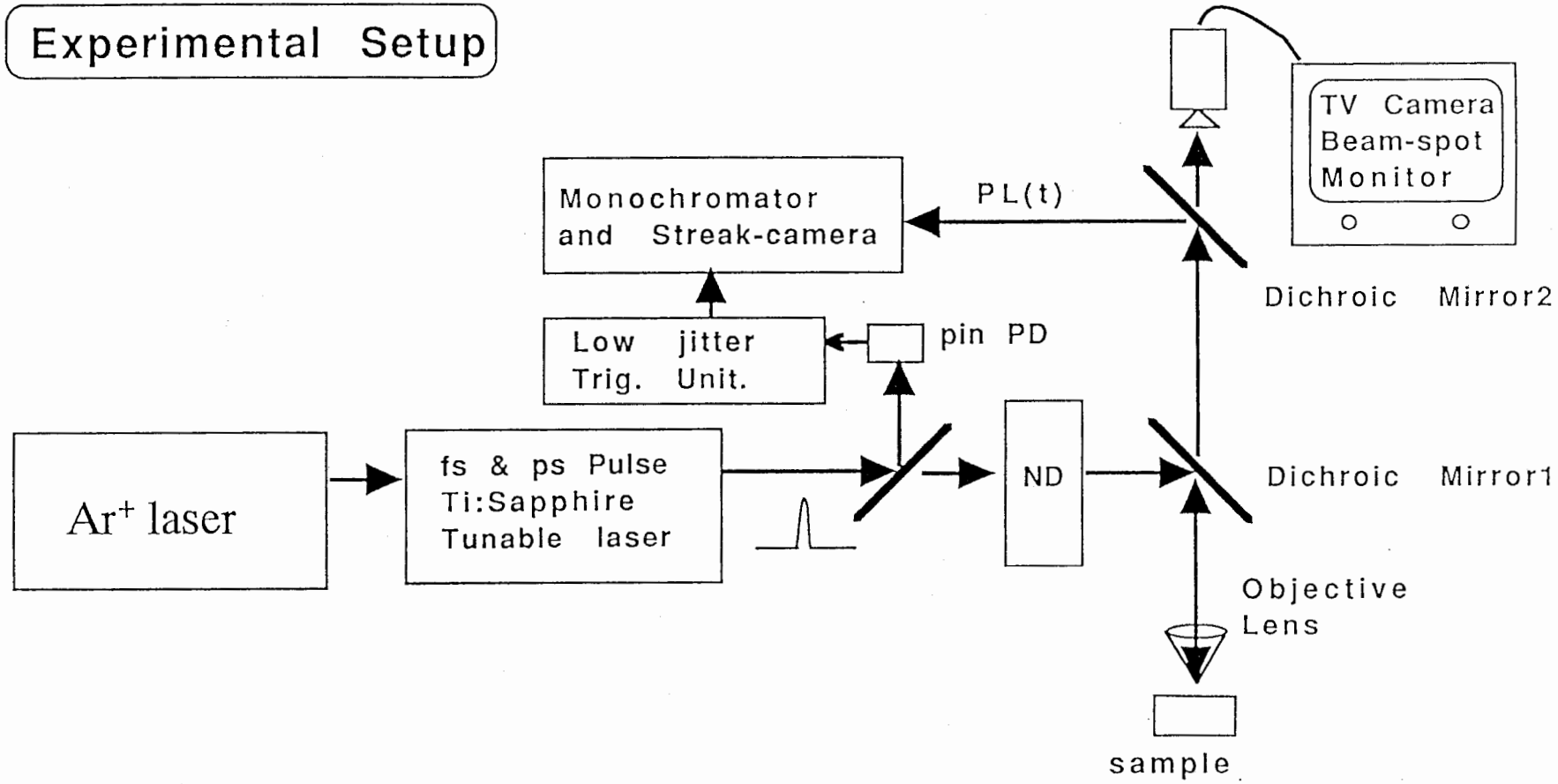

Figure 5.1: Experimental set–up used to measure time–resolved PL.

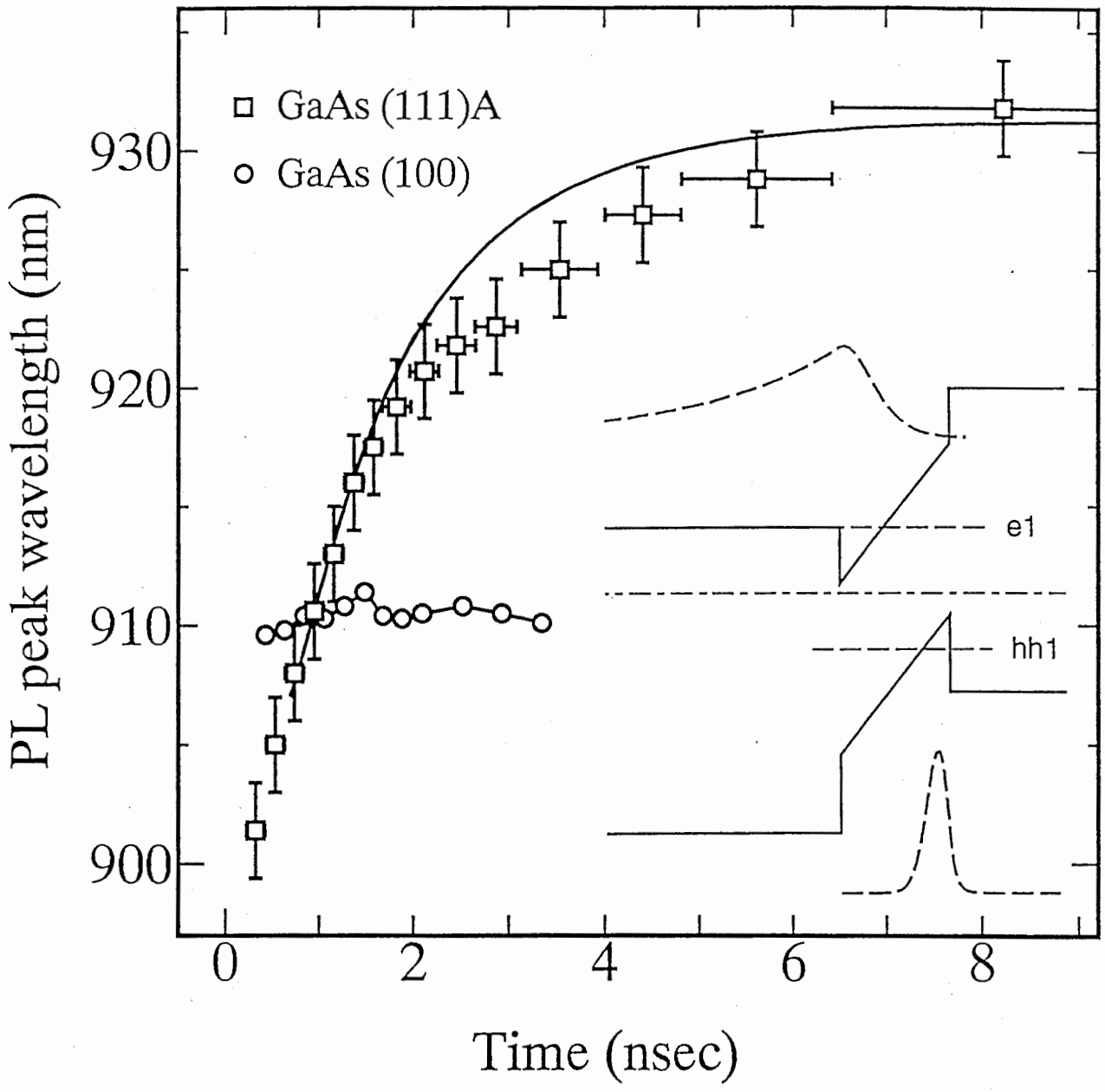

Figure 5.2: Photoluminescence peak wavelength dependence on time. The PL peak of the (111)A–oriented sample shifts toward longer wavelength as the carrier density decreases. The full line is calculated using a model described in the text. The (100)–oriented sample does not show significant change of the PL peak wavelength. The inset shows the potential profile, calculated electron and hole energy levels, and wave functions when there is not photocarriers screening the piezoelectric field in the (111)A–oriented sample. The band gap is not at the same scale of the well depths in sake of clarity.

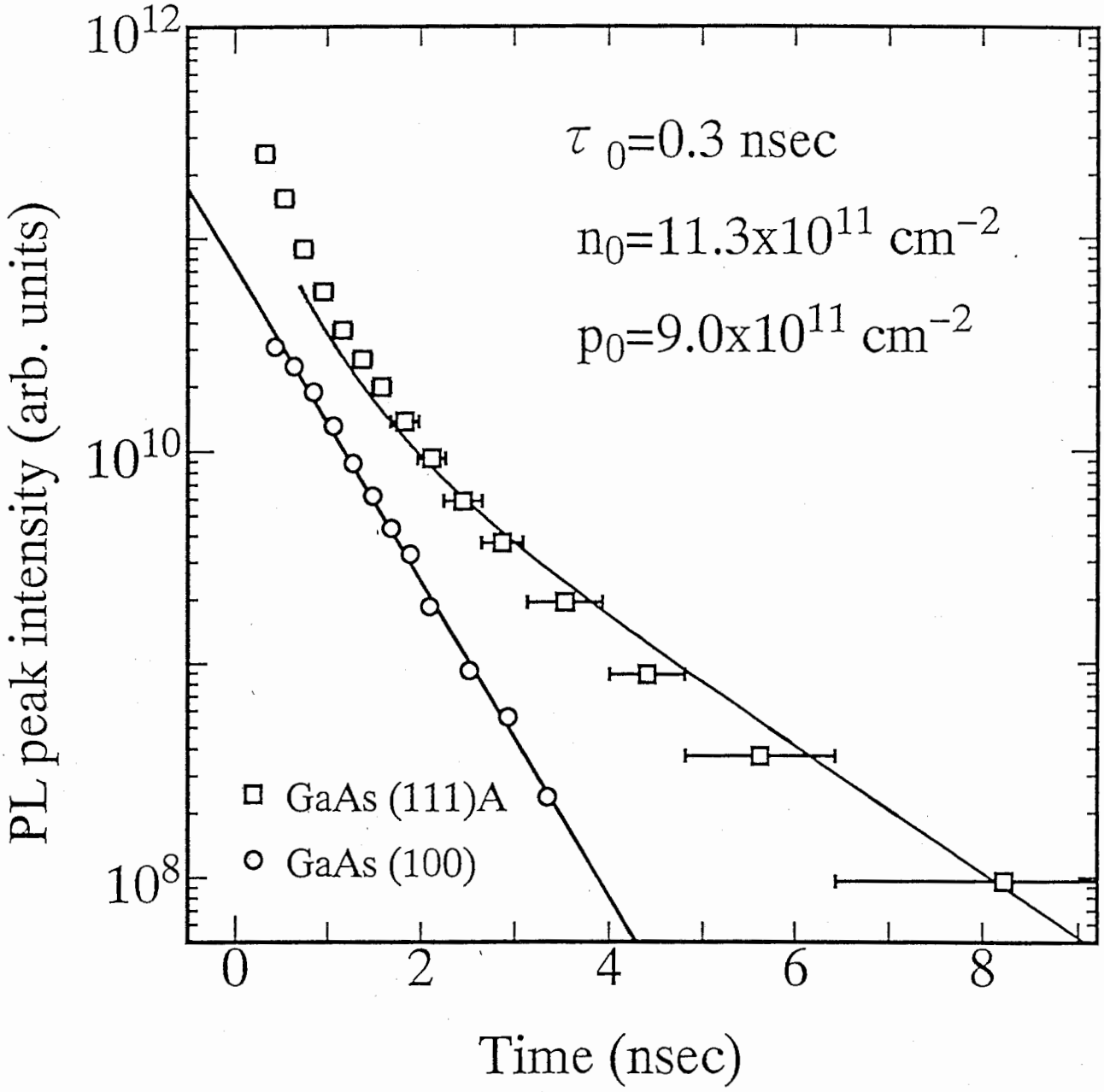

Figure 5.3: Photoluminescence peak intensity decay. The PL peak of the (111)A–oriented sample shows a non–exponential decay. The full line is calculated accordingly to a model described in the text using the parameters included in the figure. The PL peak of the (100)–oriented sample shows the usual mono–exponential decay.

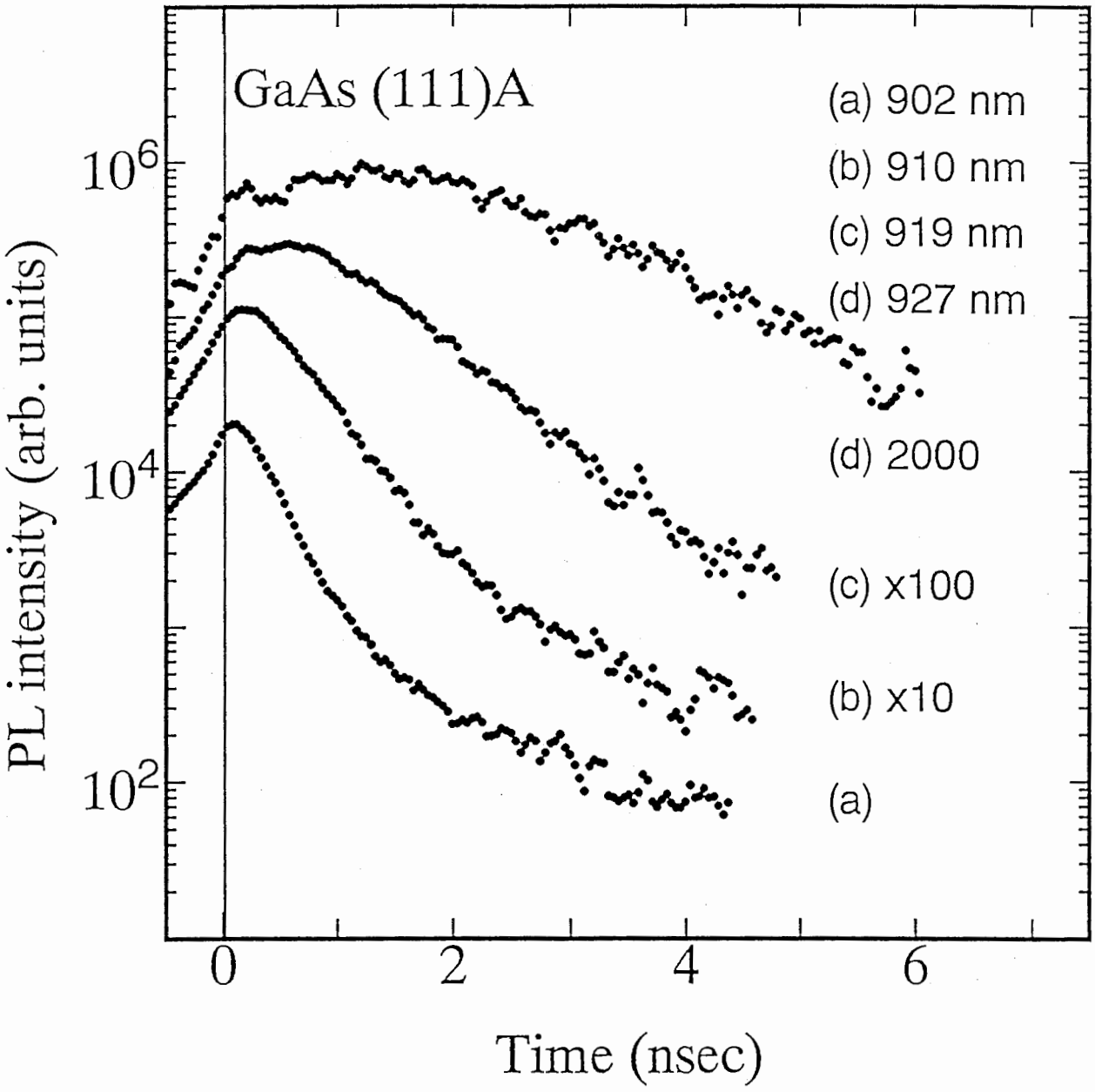

Figure 5.4: Photoluminescence intensity decay measured at various wavelengths. The short wavelength curves (a), (b) show short decay time constants. The long wavelength curves (c), (d) show a initial increase of intensity followed by a slow decay.

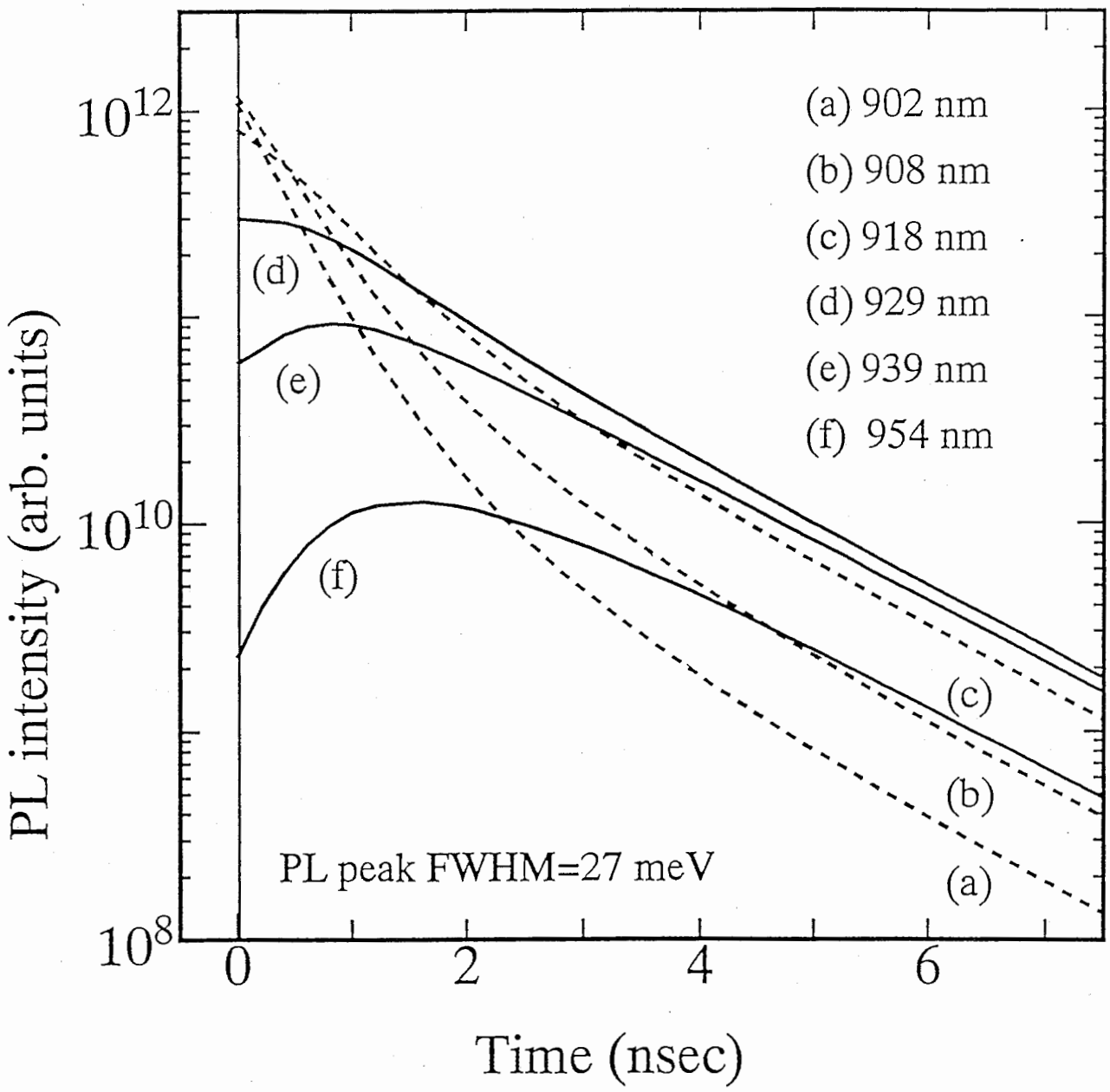

Figure 5.5: Photoluminescence intensity decay calculated at various wavelengths accordingly to the model described in the text. The features observed in the curves of Fig. 5.4 are succesfully reproduced.

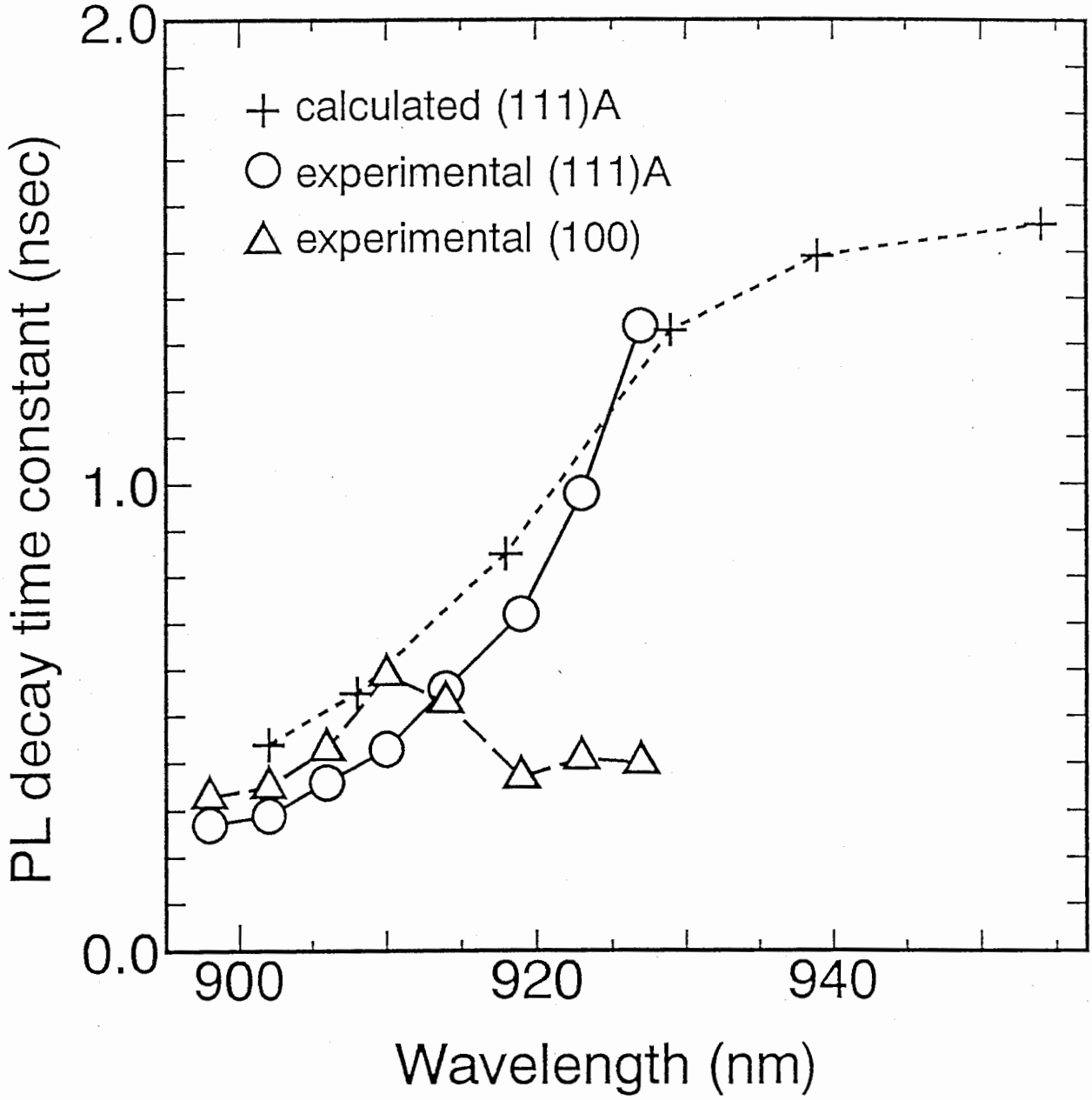

Figure 5.6: Dependence on wavelength of the experimental and calculated PL decay time constants for (111)A–oriented samples. The result for (100)–oriented samples is shown for comparison.

Chapter VI

General conclusions and future research

Our research made clear that InGaAs strained-layer heterostructures grown on GaAs substrates with orientation different from (100) display some new phenomena that have potential application to devices. In particular, the piezoelectric effect produces a strong built-in electric field inside the quantum wells and perpendicular to their interfaces that modifies the energy levels and wave functions. We show for the first time the influence of the piezoelectric effect in InGaAs quantum wells grown on GaAs (311)A-oriented substrates[1]. We also show for the first time the controllability of the optical transition energy in InGaAs quantum wells grown on GaAs (111)A-oriented substrates by applying an external voltage[2]. Finally, we demonstrate the influence of the piezoelectric field in the carrier dynamics and the enhancement of nonlinear optical properties.

We found that crystal growth mechanisms and strain relaxation mechanisms are intimately related when growing InGaAs strained layers on GaAs (111)A-oriented substrates. Strain relaxation starts well below the critical thickness predicted by the usual theory and dislocation-free layers probed to be difficult to grow[3),4)]. On the other hand, high quality strained layers where obtained routinely on GaAs (311)A and (411)A-oriented substrates. Moreover, quantum wells grown on GaAs (311)A-oriented substrates used as active layer in laser diodes showed an enhanced radiative recombination rate as compared to the (100)-oriented ones[5].

To conclude, we would like to suggest some directions for future research in these interesting topics.

The quality of quantum wells grown on GaAs (111)A-oriented substrates is not good enough for device applications. A thorough and systematic research on the growth mechanism of InGaAs layers grown on (111)A-oriented and slightly misoriented substrates would be very useful. If high quality layers are obtained, a MODFET using the 2-DEG induced by the piezoelectric effect proposed in Chapter I and the bistable device proposed in Chapter IV would be feasible.

Higher indium concentrations in the strained layers grown on high-index substrates will allow also the study of spontaneous formation of nanostructures[6]. These nanostructures will not only be affected by the component of the piezoelectric field perpendicular to the substrate but also by the in-plane component. Stronger influence of the piezoelectric effect can be expected in nanostructures grown on (311)A and (411)A oriented substrates as compared to quantum wells.

Devices based on nonlinear properties of the optical media, as the one proposed in Chapter IV, would be benefited by the higher exciton binding energies

and lower density of states predicted for these nanostructures.

References to chapter VI

1) P. O. Vaccaro, M. Takahashi, K. Fujita and T. Watanabe: Jap. J. Appl. Phys. **34** (1995) L13.
2) P. O. Vaccaro, K. Tominaga, M. Hosoda, K. Fujita and T. Watanabe: Jap. J. Appl. Phys. **34** (1995) 1362.
3) P. O. Vaccaro, M. Takahashi, K. Fujita and T. Watanabe: J. Appl. Phys. 76 (1994) 8037.
4) P. O. Vaccaro, M. Takahashi, K. Fujita and T. Watanabe: accepted for publication in J. Crystal Growth (1995).
5) M. Takahashi, P. O. Vaccaro, K. Fujita and T. Watanabe: Appl. Phys. Lett. **66** (1995) 93.
6) P. O. Vaccaro, M. Hirai, K. Fujita and T. Watanabe: Quantum Electronics and Laser Sciences'95, May 21–26, 1995, Baltimore, U.S.A.

Table I

Material parameters used in the calculations

Parameter (units)	GaAs	InAs
Lattice constant		
a_0 (Å)	5.6536	6.059
Elastic constants		
C_{11} ($x10^{11}$ dyn/cm^2)	11.88	8.33
C_{12} ($x10^{11}$ dyn/cm^2)	5.38	4.53
C_{44} ($x10^{11}$ dyn/cm^2)	5.94	3.56
a (eV)	−9.8	−5.9
b (eV)	−1.7	−1.8
d (eV)	−5.2	−3.6
Effective masses		
m^*_e/m_0	0.067	0.023
$m^*_{hh(100)}/m_0$	0.34	0.38
$m^*_{hh(111)}/m_0$	0.9	0.91
$m^*_{hh(311)}/m_0$	0.46	0.46
m^*_{lh}/m_0	0.08	0.058
$m^*_{lh(311)}/m_0$	0.09	0.09
Piezoelectric constant		
e_{14}	−0.16	−0.045
Dielectric constant		
K	12.91	15.15

Acknowledgments

I wish to express my appreciation to President Hideyuki Inomata of ATR Optical and Radio Communications Laboratories for his encouragement throughout this work. Also I would like to thank Prof. Hiroyuki Matsunami from Kyoto University for critical reading and suggestions of a part of this work, Dr. Toshihide Watanabe for valuable suggestions and discussions, Eng. Kazuhisa Fujita and Eng. Makoto Hosoda for critical reading of my manuscripts, Eng. Kouji Tominaga for teaching me to process the *pin* diodes, Eng. Mitsuo Takahashi for his cooperative approach to research, Eng. Hajime Ohnishi and Eng. Manabu Hirai for his excellent disposition to help every time that I asked for anything.